

1 Heterogeneous glacier thinning patterns over the last 40 2 years in Langtang Himal

3

4 S. Ragettli^{1,2}, T. Bolch^{2,3} and F. Pellicciotti^{1,4}

5 [1]{Institute of Environmental Engineering, ETH Zürich, Switzerland}

6 [2]{University of Zurich, Department of Geography, Zurich, Switzerland}

7 [3]{Institute for Cartography, Technische Universität Dresden, Dresden, Germany}

8 [4]{Northumbria University, Department of Geography, Newcastle upon Tyne, UK}

9 Correspondence to: S. Ragettli (ragettli@ifu.baug.ethz.ch)

10

11 Abstract

12 Himalayan glaciers are on average losing mass at rates similar to glaciers elsewhere, but
13 heavily debris-covered glaciers are receding less than debris-free glaciers or have stable
14 fronts. Hence, there is a need for multi-temporal elevation change and mass balance data to
15 determine whether glacier wastage of debris-covered glaciers is accelerating. Here, we present
16 volume and mass changes of seven glaciers (five partially debris-covered, two debris-free) in
17 the upper Langtang catchment in Nepal using a digital elevation model (DEM) from 1974
18 stereo Hexagon satellite data and seven DEMs derived from 2006-2015 stereo or tri-stereo
19 satellite imagery (e.g. SPOT6/7). The availability of multiple independent DEM differences
20 allows identifying a robust signal and narrowing down the uncertainty about recent volume
21 changes. The volume changes calculated over several multi-year periods between 2006 and
22 2015 consistently indicate that glacier thinning has accelerated with respect to the period
23 1974-2006. We calculate an ensemble-mean elevation change rate of $-0.45 \pm 0.18 \text{ m a}^{-1}$ for
24 2006-2015, while for the period 1974-2006 we identify a rate of $-0.24 \pm 0.08 \text{ m a}^{-1}$. However,
25 the behavior of glaciers in the study area is heterogeneous, and the presence of debris does not
26 seem to be a good predictor of surface mass balance trends. Debris-covered tongues have
27 spatially non-linear thinning profiles, and we show that recent accelerations in thinning
28 correlate with the presence of supraglacial cliffs and lakes. At stagnating glacier areas near the
29 glacier front, on the other hand, thinning rates decreased with time or remained constant. The

1 April 2015 Nepal earthquake triggered large avalanches in the study catchment. Two post-
2 earthquake DEMs from May and October 2015 allow quantifying the associated impact on
3 glaciers. The remaining avalanche deposit volumes six months after the earthquake are
4 negligible in comparison to 2006-2015 elevation changes. However, the deposits compensate
5 about 40% the mass loss of debris-covered tongues of one average year.

6 **1 Introduction**

7 Global warming has caused widespread recent glacier thinning and retreat in the Himalayan
8 region (Bolch et al., 2012). The impact of current and future glacier changes on Himalayan
9 hydrology and downstream water supply strongly depends on the rate of such changes.
10 However, planimetric and volumetric glacier changes are difficult to characterize due to
11 limited data availability, and many recent studies have highlighted the spatially heterogeneous
12 distribution of glacier wastage in the Himalayas (Fujita and Nuimura, 2011; Bolch et al.,
13 2012; Kääb et al., 2012). Prominent examples of current-day regional differences in glacier
14 evolution across the Hindu Kush–Karakoram–Himalaya (HKH) are the reported positive
15 glacier mass balances in the Pamir and Karakoram. Glaciers in the rest of the HKH are
16 thinning and receding (Bolch et al., 2012; Kääb et al., 2012; Gardelle et al., 2013). Across
17 regions, differences in recent glacier evolution can often be associated to differences in
18 climatic regimes (Fujita, 2008), particularly to the varying influence of the south Asian
19 monsoon and westerly disturbances (Yao et al., 2012). However, also within the same
20 climatic region the rate of glacier changes can be heterogeneous (Scherler et al., 2011b). A
21 main focus of current research is on the effect of supraglacial debris-cover on glacier response
22 to climate. Thick debris cover is a common feature in the HKH (Scherler et al., 2011b;
23 Racoviteanu et al., 2015) and a homogenous layer of thick debris effectively reduces melt
24 rates of underlying ice (e.g. Östrem, 1959; Mattson et al., 1993). However, the
25 characterization of debris-covered glacier response to climate is complicated by the frequent
26 occurrence of ice cliffs and supraglacial lakes. At exposed cliffs, melt rates are much higher
27 compared to the ice covered by a thick debris mantle (Sakai et al., 1998, 2002; Immerzeel et
28 al., 2014a; Steiner et al., 2015; Buri et al., 2016), and also at supraglacial ponds energy
29 absorption is several times larger than that at the surrounding debris-covered surface (Sakai et
30 al., 2000; Miles et al., 2016a). Recent large-scale geodetic studies based on remote sensing
31 have provided evidence that the present-day surface lowering rates of some debris-covered
32 areas in the HKH might be similar to those of debris-free areas even within the same

1 altitudinal range (Kääb et al., 2012; Nuimura et al., 2012; Gardelle et al., 2013), and surmise
2 this could be due to enhanced melt from exposed ice cliffs and supraglacial lakes. Several
3 detailed modelling studies on the other hand have provided evidence for a melt reducing
4 effect of debris at the glacier scale (e.g. Juen et al., 2014; Ragettli et al., 2015), and have
5 shown how supraglacial debris prolongs the response of the glacier to warming (Banerjee and
6 Shankar, 2013; Rowan et al., 2015). Discrepancies between the different conclusions may be
7 associated to glacier samples that are not comparable or to model uncertainties (particularly
8 regarding the representation of the effect of supraglacial cliffs and lakes on total melt).
9 Models can also provide actual melt rates while geodetic studies only provide glacier thinning
10 rates, which are affected by glacier emergence velocity.

11 Programs to monitor debris-covered glaciers have been initiated in the Karakorum (e.g.
12 Mayer et al., 2006; Mihalcea et al., 2006, 2008) and in the Central Himalaya (e.g. Pratap et
13 al., 2015; Ragettli et al., 2015). However, due to the logistical and financial constraints, long-
14 term mass balance measurements are basically inexistent in the HKH. To document changes
15 in debris-covered glacier thinning over time, declassified high-resolution reconnaissance
16 satellite data available from the 1960s and 1970s are an important source of information. In
17 the Khumbu region in the Nepalese Himalaya, Bolch et al. (2008, 2011) have calculated
18 multi-decadal mass loss of glaciers since 1962. They found that volume loss has possibly
19 increased in recent years (e.g. volume loss rates of Khumbu glacier 1970-2007: $-0.30 \pm$
20 0.09 m a^{-1} , 2002-2007: $-0.50 \pm 0.52 \text{ m a}^{-1}$). Similar conclusions were drawn by Nuimura et al.
21 (2012) who calculated accelerated thinning rates in the same study region comparing the two
22 periods 1992-2008 (e.g. Khumbu glacier: $-0.35 \pm 0.20 \text{ m a}^{-1}$) and 2000-2008 ($-0.76 \pm 0.52 \text{ m}$
23 a^{-1}).

24 A common problem of previous multi-temporal geodetic studies is the relatively low
25 statistical significance of detected changes: the uncertainties in the mass loss estimates by
26 Bolch et al. (2011) and Nuimura et al. (2012) are higher than the identified acceleration in
27 glacier thinning. The uncertainties are especially high over short periods of 21st century
28 thinning rates. For long periods with much larger absolute elevation changes, the effect of
29 DEM errors weighs less and uncertainties in glacier volume changes are lower. The aim of
30 this study is to determine changes in glacier thinning with high confidence by considering
31 multiple independent DEM differences for the 21st century. For this we use seven DEMs
32 derived from 2006-2015 stereo or tri-stereo satellite imagery and one DEM obtained from

1 1974 stereo Hexagon satellite data. We obtain an ensemble of multi-annual elevation changes
2 that provides a range of plausible values for the period between October 2006 and October
3 2015. We then assess if the elevation changes between different overlapping periods between
4 2006 and 2015 show similar characteristics. If this is the case, the ensemble of results can be
5 used to identify statistically significant changes in volume loss rates with respect to the longer
6 period 1974-2006.

7 This study presents volume and mass changes of seven glaciers (five partially debris-covered,
8 two debris-free) in the upper Langtang catchment in Nepal. The 30 m resolution dataset of
9 multi-temporal glacier volume changes allows addressing three main research questions. First,
10 we assess if overall thinning of glaciers in the region has accelerated. Second, we determine if
11 spatial thinning patterns have changed over time. To explain changes in thinning rates we
12 derive a number of glacier surface properties and glacier surface velocities. Third, we evaluate
13 if there are major differences between the response of debris-covered and debris-free glaciers
14 in the sample. Finally, we also look at the cryospheric impact of the April 2015 Nepal
15 earthquake (7.8 magnitude, epicenter approximately 80 km west of the Langtang Valley). The
16 earthquake devastated large parts of the Langtang catchment by triggering large avalanches
17 (Kargel et al., 2016). Two post-earthquake DEMs from May and October 2015 are used to
18 quantify the impact of the avalanche events on the mass balance of the debris-covered glacier
19 tongues and assess its significance in comparison to multi-annual volume changes.

20

21 **2 Study Site**

22 We analyze the seven largest glaciers in the Langtang valley (Langtang, Langshisha,
23 Shalbachum, Lirung, Ghanna, Yala, Kimoshung), located in the monsoon-dominated Central
24 Himalaya in Nepal, approximately 50 km north of Kathmandu and 100 km west of the
25 Everest region. While Yala and Kimoshung Glaciers are debris-free glaciers, all other studied
26 glaciers have tongues that are almost entirely covered by supraglacial debris (Figure 1).
27 Langtang Glacier is the largest glacier in the valley with an area of 46.5 km² in 2006 (Table 1)
28 and a total length of approximately 18 km. The smallest glacier is Ghanna Glacier with an
29 area of 1.4 km².

30 Critical debris thicknesses leading to a reduction of melt rates are exceeded over most parts of
31 the debris-covered glacier area (Ragettli et al., 2015). Relatively thin debris appears only at
32 the transition zone between accumulation and ablation area. However, at Lirung, Shalbachum,

1 Ghanna and Langshisha Glaciers the upper margins of debris-covered sections are located at
2 the foot of steep cirques and icefalls, and transition zones are therefore very short. Ice cliffs
3 and supraglacial ponds increase the heterogeneity of glacier surface characteristics in the
4 Langtang valley (Pellicciotti et al., 2015).

5 The ablation season of glaciers in the Langtang valley lasts from April to September. The
6 monsoon season (mid June – September) is at the same time the warmest and the wettest
7 period of the year. Snow cover at the lower elevation of debris-covered glaciers is common
8 only in winter (December – March). However, outside the monsoon period precipitation is
9 limited and winters are rather dry (Collier and Immerzeel, 2015).

10

11 **3 Data and methods**

12 **3.1 Satellite imagery**

13 Multitemporal high-resolution data from different sensors are applied to assess glacier change
14 in the upper Langtang catchment. Each type of remote sensing data employed to calculate
15 glacier elevation changes is listed below. Spatial and radiometric resolutions and base to
16 height (b/h) ratios are provided in Table 2.

- 17 • The oldest data originate from Hexagon KH-9 stereo satellite images from November
18 1974 (Surazakov and Aizen, 2010; Pieczonka et al., 2013; Maurer and Rupper, 2015).
19 These are declassified images from a US reconnaissance satellite program (Burnett,
20 2012).
- 21 • Cartosat-1 is a remote sensing satellite built by the Indian Space Research
22 Organisation (Tiwari et al., 2008). We purchased radiometrically corrected along-track
23 stereo imagery (processed at level ‘ortho-kit’) of the upper Langtang catchment from
24 October 2006 and November 2009. Cartosat-1 data have been previously used for
25 DEM generation e.g. in the Khumbu region in the Nepal Himalaya by Bolch et al.
26 (2011) and Pieczonka et al. (2011).
- 27 • ALOS-PRISM (Advanced Land Observing Satellite - Panchromatic Remote-Sensing
28 Instrument for Stereo Mapping) was an optical sensor mounted on a Japanese satellite
29 system which operated from January 2006 to April 2011 (Bignone and Umakawa,
30 2008; Tadono and Shimada, 2009; Lamsal et al., 2011; Holzer et al., 2015). We

1 purchased a radiometrically calibrated along-track triplet mode scene from December
2 2010.

- 3 • SPOT6/7 (Système pour l’Observation de la Terre) along-track tri-stereo images
4 were acquired upon request in April 2014, May 2015 and October 2015. SPOT6 and 7
5 are the newest satellites of the SPOT series which have been frequently used for
6 geodetic glacier mass balance studies (e.g. Berthier et al., 2007, 2014; Pieczonka et al.,
7 2013). We acquired stereoscopic images in panchromatic mode corrected for
8 radiometric and sensor distortions. Two of the three SPOT6/7 scenes used in this study
9 were acquired in April/May which means that limited amounts of winter snow is still
10 present on the images. However, the imagery has a high spation resolution (1.5 m) and
11 high radiometric depth of 12bit which leads to good correlation results also over
12 snowy parts.
- 13 • Overlapping pairs of high-resolution images acquired by the WorldView-2 and 3
14 satellites in February 2014 provide the basis of 8m DEMs downloaded from
15 <http://www.pgc.umn.edu/elevation> (Noh and Howat, 2015).

16 **3.2 DEMs and elevation changes**

17 **3.2.1 DEM generation**

18 The Hexagon DEM used here was generated for the study by Pellicciotti et al. (2015). We
19 therefore refer to this study for further technical details regarding the Hexagon DEM. The
20 SPOT6/7, Cartosat-1 and ALOS PRISM DEMs were generated for this study using the
21 OrthoEngine module of PCI Geomatica 2015. We used the same parameters for DEM
22 generation as proposed by Berthier et al. (2014) except setting the parameter ‘DEM detail’ to
23 ‘very high’ instead of ‘low’, which provided better results for the rugged debris-covered
24 glacier surfaces. The basis for the georectification were six differential GPS (dGPS) points
25 collected on Lirung Glacier on 23 October 2014 (Brun et al., 2016). Because glacier motion
26 and ablation have to be accounted for when using on-glacier dGPS points, we first generated a
27 DEM from an across-track Pléiades stereo image pair from 1 and 9 November 2014 using the
28 available dGPS points as ground-control points (GCPs). Glacier melt between 23 October and
29 the acquisition dates of the Pléiades scenes is negligible due to the low temperatures during
30 this period. The horizontal shift due to glacier motion during this period is less than the grid

1 size of the Pléiades image (0.5 m) and is therefore also negligible. Subsequently, we
2 determined 17 GCPs on the basis of the Pléiades scene which were then used to derive a
3 DEM from the SPOT6 April 2014 tri-stereo scene. The Pléiades DEM itself is not used in the
4 following to calculate glacier elevation changes since it covers only a small part of the
5 catchment and since only low stereo matching scores were achieved at elevations higher than
6 4300 m a.s.l. due to snowfall onset between 1 and 9 November 2014. To guarantee high
7 quality GCPs, only pixels with correlation scores higher than 0.7 were considered for GCPs.
8 Since the Pléiades scene covers only about one fourth of the upper Langtang catchment, an
9 additional 60 GCPs were determined on the basis of the April 2014 SPOT6 scene for the
10 DEM extraction from the Cartosat-1, ALOS Prism and SPOT7 scenes. In addition to the
11 GCPs, approximately 100 tie points for each scene were used to match stereo pairs before
12 DEM extraction.

13 The WorldView DEMs are 8m posting Digital Elevation Models (DEMs) produced using the
14 Surface Extraction with TIN-based Search-space Minimization (SETSM) by Noh and Howat
15 (2015). The WorldView DEMs rely on the satellite positioning model to locate the surface in
16 space. The scenes from February 2015 which provide the basis of the two WorldView DEMs
17 used in this study were acquired only 20 days apart (Table 2) and are adjacent to each other.
18 The Worldview-2 DEM covers the western part of the study catchment and the WorldView-3
19 DEM the eastern part. Those DEMs were merged for this study and in the following are
20 referred to as one single DEM representative of February 2015.

21 In addition to the DEMs discussed above, the 2000 SRTM (Shuttle Radar Topography
22 Mission) 1 Arc-Second Global DEM (30 m spatial resolution) was used to calculate slopes
23 and accumulation area ratios (AARs) of glaciers (Table 1) and to define 50 m altitude bands.
24 However, the SRTM DEM was not used for DEM differencing because of the uncertainty
25 regarding the penetration depth of the radar signal into snow and ice (Gardelle et al., 2013;
26 Kääb et al., 2015; Pellicciotti et al., 2015). Only DEMs extracted from optical stereo imagery
27 are therefore employed to calculate elevation changes in this study.

28 **3.2.2 Co-registration and DEM differencing**

29 We considered all possible DEM pairs to measure the glacier elevation changes. The number
30 of possible two-fold combinations of n DEMs is

$$1 \quad N_{\Delta t} = \sum_{k=1}^{n-1} k, \quad (1)$$

2 Elevation differences over $N_{\Delta t} = 28$ different time periods can therefore be calculated from
3 the eight available DEMs extracted from optical stereo imagery. Co-registration of each
4 DEM-pair is applied in order to minimize the errors associated with shifts. Systematic errors
5 in the elevation change maps due to tectonic uplift which could be relevant after the April
6 2015 Nepal earthquake are also corrected with the co-registration. For this purpose we
7 exclude from each DEM the non-stable terrain such as glaciers and in general all off-glacier
8 area at elevations higher than 5400 m a.s.l. (which is the estimated equilibrium line altitude
9 (ELA) in the Upper Langtang catchment (Ragettli et al., 2015)). The correlation score maps,
10 indicating which pixels have been matched successfully during the DEM extraction process,
11 are used to exclude all DEM grid cells with a correlation score below 0.5. Then, horizontal
12 shifts are determined by minimizing the aspect-dependent bias of elevation differences (Nuth
13 and Kääb, 2011) between each DEM pair. Because of the slope dependency of the method all
14 terrain below a slope of 10° is excluded. The ‘older’ DEM is then resampled (bilinear
15 interpolation) according to the determined horizontal shift. In a second step the vertical DEM
16 shifts and possible tilts are corrected using second order trend surfaces fitted to all gently
17 inclined ($\leq 15^\circ$) stable terrain (Bolch et al., 2008; Pieczonka et al., 2011; Pieczonka and Bolch,
18 2015).

19 We resample all DEMs bilinearly to the grid size of the coarsest DEM (30 m) to reduce the
20 effect of different resolutions. Elevation differences are calculated by subtracting the older
21 from the younger DEM (such that glacier thickening values are positive) and are converted to
22 elevation change rates by dividing by the number of ablation seasons between the acquisition
23 dates. Seasonal effects on elevation change rates are neglected when discussing time intervals
24 between DEMs of 4 years or longer, since elevation changes during the winter half-year are
25 usually minor (less than 20% of annual precipitation during post-monsoon and winter;
26 Immerzeel et al., 2014b; and less than 3% of annual glacier ice-melt; Ragettli et al., 2015).
27 Area-average glacier elevation change rates are calculated using always the maximum glacier
28 extent between two acquisition dates.

1 3.2.3 Processing of elevation change maps

2 Processing of the elevation change ($\Delta h/\Delta t$) maps involves two main steps: i) removal of pixel
3 values identified as outliers and ii) filling of gaps.

4 Outlier removal

5 The stereo matching score maps provided by PCI Geomatica are used to identify elevation
6 data that can be considered for elevation change calculations. If the correlation score of a
7 given DEM pixel is below 0.5, this indicates a poor matching score (Pieczonka et al. 2011)
8 and therefore the corresponding $\Delta h/\Delta t$ values are treated as 'no data'. Very unrealistic
9 elevation change data (exceeding ± 150 m) are also excluded from the analysis.

10 We use the standard deviation (σ) of observed elevation changes to identify $\Delta h/\Delta t$ outliers.
11 Outliers are defined separately for debris-covered glacier areas and debris-free glacier areas.
12 For the latter we additionally distinguish between glacier area below and above the ELA
13 (estimated at 5400 m a.s.l., see above). σ -levels are thus calculated for each of the three area
14 types in every $\Delta h/\Delta t$ map. Below the ELA (both debris-free and debris-covered area), pixels
15 are defined as outliers if $\Delta h/\Delta t$ values differ from the average by $>3\sigma$ (e.g. Gardelle et al.,
16 2013). This means that only very few data are classified as outliers, since three standard
17 deviations account for 99.7% of the sample (assuming the distribution is normal). The
18 conservative outlier definitions are justified by the shallow slopes and high contrast, which
19 also explains why stereo matching scores are generally higher below the ELA (Figure 2c).
20 Above the ELA, steep terrain or featureless snow surfaces lead to low DEM accuracy and
21 therefore the outlier criteria should be more restrictive (e.g. Pieczonka et al., 2013; Pieczonka
22 and Bolch, 2015). On debris-free glacier area above the ELA, pixels are therefore defined as
23 outliers if $\Delta h/\Delta t$ values differ from the average by $>1\sigma$ (which applies to approximately 32%
24 of the values if the distribution is normal). A stricter criterion for the accumulation area is also
25 justified by the fact that it can be assumed that elevation changes in the accumulation areas
26 over periods of several years are small (Schwitter and Raymond, 1993; Huss et al., 2010).
27 Because we use different σ thresholds above and below the ELA we test the sensitivity of
28 calculated glacier volume changes to a ± 100 m ELA uncertainty. Furthermore, we test the
29 sensitivity to different outlier definitions by comparing our results to the results obtained with
30 a 2σ -level applied to all area types.

31

1 Gap filling

2 On the glacier areas below the ELA, with only very few data gaps, missing data are replaced
3 using inverse distance weighting (IDW). In the accumulation areas, on the other hand, data
4 gaps can extend over a wide elevation range if the terrain is steep or if the gaps are very large.
5 Because of the elevation dependency of $\Delta h/\Delta t$ values (e.g. Huss et al., 2010) only values from
6 the same altitudinal range should be used to fill data gaps. We thus replace missing data in the
7 accumulation areas by median $\Delta h/\Delta t$ values per 50-m elevation band considering all available
8 data for a given glacier (also from $\Delta h/\Delta t$ maps representative of different periods). For this,
9 we first calculate the mean elevation change rates per 50-m elevation band of each glacier and
10 every $\Delta h/\Delta t$ map and then determine the median of the ensemble. $\Delta h/\Delta t$ maps that are
11 rejected from the ensemble (see Section 3.2.5 below) and in general all values representative
12 of short periods ($\Delta t < 4$ years) are not considered to calculate the ensemble-median values.

13 **3.2.4 Uncertainty**

14 Elevation change uncertainty estimates are based on the standard error $E_{\Delta h}$ calculated per
15 elevation band (Gardelle et al., 2013). The standard error quantifies the effect of random
16 errors on uncertainty according to the standard principles of error propagation:

$$17 \quad E_{\Delta h} = \frac{\sigma_{\Delta h, noglac}}{\sqrt{N_{eff}}} \quad (2)$$

$$18 \quad N_{eff} = \frac{N_{tot} \times PS}{2d} \quad (3)$$

19 $\sigma_{\Delta h, noglac}$ is the standard deviation of the mean elevation change of non-glacierized terrain per
20 elevation band, N_{eff} is the effective and N_{tot} the total number of observations. PS is the pixel
21 size (30 m) and d is the distance of spatial autocorrelation. d is equal to the range of the
22 spherical semivariogram obtained by least squares fit to the experimental, isotropic variogram
23 of all off-glacier elevation differences (Wang and Kääb, 2015; Magnússon et al., 2016). The
24 distance of spatial autocorrelation of the 28 elevation change maps varies between 260 m and
25 730 m with an average of 495 m.

26 To quantify the elevation change uncertainty of glacier area spanning several elevation bands,
27 weighted averages of $E_{\Delta h}$ are calculated. $E_{\Delta h}$ of each individual elevation band is weighted by
28 the glacier hypsometry. Elevation change uncertainties therefore vary for each individual

1 glacier because of the different glacier area-elevation distributions. $E_{\Delta h}$ tends to increase with
2 altitude (Figure 3, Figure 4) due to steeper slopes, snow and deep shadows, which are factors
3 that decrease the accuracy of DEMs derived from stereo data (e.g. Nuimura et al., 2011).
4 Uncertainty estimates for each individual glacier therefore account for the spatially non-
5 uniform distribution of uncertainty. Elevation change uncertainties of glaciers with a high
6 accumulation area such as Kimoshung and Lirung Glaciers (Table 1) are 50%-100% higher
7 than those of other glaciers, in accordance with lower DEM matching scores (Figure 2). The
8 low uncertainty associated to debris-covered areas agrees with the 30%-100% lower off-
9 glacier errors on shallow slopes ($s < 18^\circ$, 95th percentile of debris-covered glacier slopes) than
10 on steeper slopes ($s < 45^\circ$, 95th percentile of glacier slopes; Figure S1).

11 The standard error can be interpreted as the 68% confidence interval of the sample mean if the
12 distribution is normal. Since we are conservatively assuming no error compensation across
13 elevation bands the approximate confidence level in our uncertainty estimates per glacier is
14 higher than 68%.

15 This study aims at obtaining an ensemble of results about elevation change rates from the set
16 of seven DEMs available for the period 2006-2015 and we thus calculate an ensemble
17 uncertainty. The uncertainty in a sample mean is different from the uncertainty in individual
18 observations about recent volume change rates. To identify the range of ensemble values
19 (hereafter ‘ensemble uncertainty’) we use the standard deviation of the ensemble values
20 multiplied by 1.96. By multiplication with 1.96 we obtain 95% confidence levels, assuming
21 normal distribution.

22 For overall mass budget uncertainties we assume an ice density of 850 kg/m^3 to convert the
23 volume change into mass balance (Sapiano et al., 1998; Huss, 2013) and consider the
24 elevation change rate uncertainties and an ice density uncertainty of 60 kg/m^3 .

25 **3.2.5 Ensemble selection**

26 The 28 available $\Delta h/\Delta t$ maps are classified in two groups: maps that involve the Hexagon
27 1974 DEM and maps that represent only 21st century elevation changes (2006-2015). From
28 the first group we only use the 1974-2006 $\Delta h/\Delta t$ map, to strictly separate our two main study
29 periods 1974-2006 and 2006-2015. From the second group we consider only those maps that
30 are least affected by uncertainties. Since $\Delta h/\Delta t$ uncertainties increase with shorter time
31 intervals between DEMs (Figure 5, Table 3) and since similar elevation change patterns are

1 more likely for overlapping periods, we discard all $\Delta h/\Delta t$ maps with $\Delta t < 4$ years. In addition,
2 we discard all $\Delta h/\Delta t$ maps involving the ALOS PRISM DEM, since uncertainties associated
3 to $\Delta h/\Delta t$ maps involving this DEM are 30-100% higher than if other DEMs are involved
4 (Table 3). The ALOS-PRISM sensor has a radiometric resolution of 8-bit, which means that
5 in comparison to a 12-bit image (SPOT6/7, Table 2), $2^4=16$ times less information is provided
6 per panchromatic image pixel. The image contrast is therefore lower, which decreases the
7 accuracy of this DEM.

8 Due to the incomplete representation of Langtang Glacier on the SPOT6 Apr 2014 scene (the
9 scene does not cover the area north of $28^{\circ}19'N$), $\Delta h/\Delta t$ maps involving this DEM are
10 excluded when discussing ensemble results for Langtang Glacier.

11 We assess separately if the $\Delta h/\Delta t$ maps involving the post-earthquake DEMs (SPOT7 May
12 2015 and Oct 2015) can be considered for the 2006-2015 ensemble (section 4.1). Elevation
13 changes after the earthquake in April 2014 might be substantially different from those before
14 the earthquake because of large post-earthquake avalanches.

15 **3.3 Delineation of glaciers, debris-covered areas, and supraglacial cliffs/lakes**

16 The glacier outlines were manually delineated. We used the orthorectified satellite images
17 with the least snow cover (the Cartosat-1 2006 and 2009 scenes) to delineate the accumulation
18 areas, and assumed no changes in the accumulation area over time. The tongues of the seven
19 studied glaciers and debris extents were re-delineated for every year for which satellite images
20 are available (1974, 2006, 2009, 2010, 2014 and 2015), using the corresponding orthorectified
21 satellite images. A first operator delineated the outlines and a second operator provided
22 feedback in order to improve delineation accuracy. To quantify the uncertainty in derived
23 glacier area changes we consider a 0.5 pixel size delineation uncertainty (Paul et al., 2013).

24 The four largest glaciers in the valley were already delineated manually by Pellicciotti et al.
25 (2015) for the years 1974 and 2000. However, we decided not to use those outlines because of
26 the considerably higher resolution of the images that are available for this study and for
27 consistency in the procedure applied for different outlines. We also re-delineated the
28 catchment boundaries using the SRTM 30 m DEM and an automated flow accumulation
29 process to accurately delineate the ice divides between neighboring catchments. As a result,
30 the calculated glacier areas (Table 1) changed considerably with respect to Pellicciotti et al.
31 (2015). The 1974 glacier area of Langshisha Glacier changed by -40.4% (Figure S2), mostly

1 due to clipping with the catchment mask which reduced the extent of the accumulation areas.
2 The 1974 areas of Langtang, Shalbachum and Lirung changed by -8.7%, -9.5% and +8.0%,
3 respectively.

4 To identify glacier area associated to small glaciers in the catchment that are not discussed in
5 this study we used the glacier outlies provided by the GAMDAM glacier inventory (Nuimura
6 et al., 2015). Those areas were masked out from off-glacier terrain for the co-registration of
7 the DEMs and stable terrain accuracy assessments.

8 Six quality checked maps of supraglacial cliffs and lakes are used to characterize debris-
9 covered glacier surfaces (Steiner et al., 2016). The cliff and lake inventories were generated
10 based on the available satellite imagery for the period 2006-2015 (Oct 2006, Nov 2009, Dec
11 2010, Apr 2014, May 2015 and Oct 2015). As for the glacier outlines, cliff and lake outlines
12 have been delineated by two independent operators. To further improve the accuracy of the
13 inventories, a third operator used slope and elevation change maps to identify potential cliff
14 and lake locations. The first two operators then used these indications to review the
15 inventories. All outlines have been obtained by manual delineation on the basis of the
16 orthorectified satellite images.

17 We calculated the fraction of pixels including lakes and cliffs per 50 m elevation band of each
18 debris-covered tongue (excluding tributary branches, Figure 6). In the following, we only
19 discuss median 2006-2015 cliff and lake area fractions to minimize seasonal effects. Large
20 avalanche cones, such as those present on Lirung and Langtang Glacier after the April 2015
21 earthquake, are masked out from the inventories before calculating median values.

22 **3.4 Surface velocities**

23 To assist with the interpretation of volumetric changes, we use glacier velocities determined
24 with the COSI-Corr cross-correlation feature-tracking algorithm (Leprince et al., 2007) and
25 the available satellite imagery. The orthorectified Cartosat-1 Nov 2009 and ALOS-PRISM
26 Dec 2010 images were used for this purpose. Other image pairs were not considered due to
27 longer periods between acquisitions (leading to image decorrelation) or the presence of snow
28 patches at lower elevations (SPOT6 April 2014, SPOT7 May 2015). The selected
29 orthorectified images (5 m resolution) were adjusted according to the shifts determined by co-
30 registration (Section 3.2.2). Since the window size must be large enough to avoid correlating
31 only noise but small enough not to degrade the output resolution (Dehecq et al., 2015), we

1 tested several configurations. The best results for the COSI-Corr multiscale correlation
2 analysis were achieved using a window size of 128 down to 32 pixels, as also proposed by
3 Scherler et al. (2008). To post-process the velocity data we removed pixels with x- or y-
4 velocity values greater than 40 m/a, since these were identified as errors by manually
5 measuring the surface displacement on the basis of the orthorectified images and prominent
6 features. We then ran a median filter on the data to remove areas which show a local reversal
7 in x or y directions. Missing values were then filled with the mean of the adjacent 8 values.
8 Finally, the velocity map was resampled to 30 m resolution with a bicubic algorithm.

9 **3.5 Assessment of the April 2015 earthquake impact**

10 We quantify the impact of the avalanche events after the April 2015 earthquake on volume
11 changes of debris-covered tongues. For this purpose we use the April 2014 - May 2015 Δh
12 map to quantify the accumulated volumes less than two weeks after the earthquake, and the
13 April 2014 - Oct 2015 Δh map to quantify the remaining volumes after one ablation season.
14 To identify glacier area where avalanche material accumulated we consider all glacier grid
15 cells with significant positive elevation changes ($\Delta h > 5$ m). Approximately 7.9% (1.9 km²) of
16 all debris-covered areas were affected by avalanches according to this definition. To calculate
17 the deposited volumes we first estimate the volume loss between April 2014 and April 2015
18 (pre-earthquake), considering the mean annual thinning rates of the identified avalanche
19 affected areas between Oct 2006 and Feb 2015. We then sum these volumes with the volume
20 change measured by DEM differencing between 21 April 2014 and 7 May 2015 to obtain
21 accumulated avalanche material volumes. Note that we do not use the Feb 2015 - May 2015
22 and the Feb 2015 - Oct 2015 Δh maps to quantify avalanche debris volumes because the
23 calculated uncertainties associated to these maps are up to 300% higher than the uncertainties
24 associated to the Apr 2014 differential DEMs (Table S1).

25

26 **4 Results**

27 **4.1 Impacts of the April 2015 earthquake**

28 We calculate a total volume of post-earthquake avalanche debris in May 2015 of $2.49 \cdot 10^7$ m³,
29 which is equivalent to a cube length of 292 m. 40% of the avalanche material remained until 6
30 Oct 2015 (Table 4). The two glaciers which were most affected by avalanches were Langtang

1 Glacier (receiving 58% of the total volume) and Lirung Glacier (29%). The avalanche cone at
2 Lirung Glacier piled up to a height of nearly 60 m, while the avalanche material at Langtang
3 Glacier was more spread (Figure 7). Consequently, more material remained until 6 Oct 2015
4 at Lirung Glacier (57%), while at Langtang Glacier 31% remained (Table 4). Field visits at
5 the end of October 2015 revealed that a smooth debris layer melted out of the avalanche
6 material and covered the surface uniformly with a thickness of a few centimeters (P. Buri and
7 P. Egli, personal communication).

8 The avalanche deposits in May 2015 and those remaining in Oct 2015 are equivalent to an
9 average positive surface elevation change over all debris-covered glacier area of $1.31 \pm$
10 0.35 m and 0.52 ± 0.19 m (Table 4), respectively. A positive surface elevation change of
11 1.31 m corresponds to an average elevation change rate of approximately $0.16 - 0.26$ m a⁻¹ if
12 divided over five to eight years. This exceeds the uncertainty in $\Delta h/\Delta t$ values attributed to
13 debris-covered glacier area (± 0.12 m a⁻¹, Table 3). The May 2015 DEM will therefore not be
14 considered for the 2006-2015 ensemble. A positive elevation change of 0.52 m distributed
15 over multi-annual periods within the 2006-2015 ensemble, however, corresponds to a change
16 rate of only $0.06 - 0.09$ m a⁻¹. This impact is within the uncertainty range associated to multi-
17 annual $\Delta h/\Delta t$ values. 2006-Oct 2015 and 2009-Oct 2015 elevation change rates are thus not
18 substantially different from those before the earthquake and will be considered for the 2006-
19 2015 ensemble (Figure S3).

20 The effect of avalanche debris on Apr 2014-Oct 2015 glacier thinning profiles (Figure 8) can
21 be identified at Langtang Glacier (4500-4900 m a.s.l.), at Langshisha Glacier (4800 m a.s.l.),
22 at Shalbachum Glacier (4750 m a.s.l.) and most prominently at Lirung Glacier (4350-4400 m
23 a.s.l.). However, 2006-Oct 2015 and 2009-Oct 2015 thinning profiles are mostly within the
24 error bounds associated to other multi-annual periods shown in Figure 8.

25 **4.2 Mean glacier surface elevation changes**

26 The 2006-2015 ensemble consistently indicates an increase in mean glacier thinning rates in
27 comparison to the period 1974-2006 (Figure 9h). For 2006-2015 we calculate an ensemble-
28 mean thinning rate of -0.45 ± 0.18 m a⁻¹, while for the period 1974-2006 we identify a
29 thinning rate of -0.24 ± 0.08 m a⁻¹ (Table 5). This corresponds to an increase in determined
30 mean thinning rates by 0.21 m a⁻¹ or 87.5%. The error bounds associated to the two periods
31 are overlapping at the extremes. However, error bounds are not overlapping at 80%

1 confidence levels: multiplication of the ensemble standard deviation by 1.28 (80% confidence
2 level assuming normal distribution) instead of 1.96 (95% confidence level) results in an
3 uncertainty of $\pm 0.11 \text{ m a}^{-1}$ instead of $\pm 0.18 \text{ m a}^{-1}$. The probability that 2006-2015 elevation
4 changes are higher than $-0.45 + 0.11 \text{ m a}^{-1} = -0.34 \text{ m a}^{-1}$ is thus 10%. Assuming a probability
5 of less than 10% that 1974-2006 elevation changes are below this value, the estimated
6 confidence level of accelerated thinning rates is higher than 99%.

7 From the seven studied glaciers in the valley, the thinning rates of Langtang, Langshisha and
8 Yala Glaciers have accelerated at 99% confidence levels (Figure 9, Table 5). At Shalbachum
9 Glacier the error bounds are overlapping but the estimated probability that 1974-2006
10 thinning rates are higher than 2006-2015 volume loss rates is less than 10%. At Lirung and
11 Kimoshung Glaciers the mean thinning rates have likely remained approximately constant:
12 the 2006-2015 ensemble mean and the value for 1974-2006 differ by 0.05 m a^{-1} and 0.08
13 m a^{-1} , respectively (Table 5). The estimated probability that at one of these glaciers mean
14 thinning rates changed by less than $\pm 0.15 \text{ m a}^{-1}$ between the two periods is higher than 90%.
15 Also at Ghanna Glacier the 1974-2006 value and the 2006-2015 ensemble mean differ by
16 only 0.05 m a^{-1} (Table 5). However, the scatter in the 2006-2015 values is such that no trend
17 can be identified. The ensemble uncertainty is $\pm 0.43 \text{ m a}^{-1}$, which is higher than at any other
18 glacier (Table 5). Ghanna Glacier is also the only glacier where the ensemble of values
19 available for the period 2006-2015 did not narrow down the uncertainty associated to
20 individual periods (Figure 9).

21 The most negative elevation change for 1974-2006 was observed at Shalbachum (-0.43 ± 0.08
22 m a^{-1} , Table 5) and Ghanna Glacier ($-0.51 \pm 0.05 \text{ m a}^{-1}$). The least negative values were
23 calculated for Langshisha ($-0.12 \pm 0.09 \text{ m a}^{-1}$) and Kimoshung Glaciers ($0.06 \pm 0.13 \text{ m a}^{-1}$).
24 Comparing the period 1974-2006 and the 2006-2015 ensemble mean values, the strongest
25 thinning acceleration took place at Yala Glacier (from $-0.33 \pm 0.06 \text{ m a}^{-1}$ to $-0.89 \pm 0.23 \text{ m a}^{-1}$,
26 Table 5). Yala Glacier was also the glacier with the highest 2006-2015 ensemble mean
27 thinning rate.

28 Volume change rates are also calculated separately for the five debris-covered tongues
29 (Figure 10, Table 5). An increase in identified mean volume loss rates is evident on the
30 Langtang, Langshisha, Shalbachum and Lirung tongues. Thinning rates increased between
31 15% (Langtang tongue) and 68% (Langshisha and Shalbachum tongues). For Ghanna tongue
32 the identified changes in thinning rates are not significant given the uncertainties, but five out

1 of six members of the 2006-2015 ensemble suggest that thinning rates have more likely
2 decreased rather than accelerated.

3 Of all debris-covered areas, the downwasting rates on Lirung tongue are the highest. This
4 applies to both the period 1974-2006 ($-1.03 \pm 0.05 \text{ m a}^{-1}$, Table 5) and to the 2006-2015
5 ensemble mean ($-1.67 \pm 0.59 \text{ m a}^{-1}$, Table 5). The 2006-2015 ensemble uncertainty is very
6 large on Lirung tongue ($\pm 0.59 \text{ m a}^{-1}$), which we believe is due to systematic errors in the
7 2009-2014 differential DEM that represents an outlier in the ensemble (Figure 10). However,
8 neither on Lirung nor on Langtang tongue (the two glaciers most affected by post-earthquake
9 avalanches, see Section 4.1) post-earthquake elevation changes (2006-Oct 2015 or 2009-Oct
10 2015) represent outliers with respect to other 2006-2015 multi-annual periods. The lowest
11 volume loss rates are identified for Ghanna tongue (Figure 10, Table 5). Here, the 2006-2015
12 ensemble mean value ($-0.50 \pm 0.20 \text{ m a}^{-1}$) indicates more than three times lower thinning rates
13 than at Lirung tongue.

14 **4.2.1 Sensitivity to outlier correction and ELA definitions**

15 Mean elevation change values are most sensitive to outlier definitions for Langshisha Glacier
16 1974-2006 (Table 6). If a 2σ -level is used to define outliers for all area types (instead of a 3σ -
17 level above and a 1σ -level below the ELA, Section 3.2.3), $\Delta h/\Delta t_{1974-2006}$ for Langshisha
18 Glacier changes by -0.09 m a^{-1} from $-0.12 \pm 0.09 \text{ m a}^{-1}$ to $-0.21 \pm 0.09 \text{ m a}^{-1}$. If we compare
19 the results obtained with an estimated ELA at 5300 m a.s.l. to the results obtained with an
20 ELA at 5500 m a.s.l., mean elevation changes of individual glaciers differ by up to -0.23 m a^{-1}
21 (Shalbachum Glacier 1974-2006). However, only for two glaciers the sensitivity values
22 exceed the uncertainty values estimated from off-glacier elevation change errors (at
23 Shalbachum and Yala Glacier 1974-2006, Table 6). In both cases the differences can be
24 explained by unrealistic patterns (strongly negative elevation changes above 5400 m a.s.l.),
25 that are not identified as outliers with a 3σ threshold applied to areas below 5500 m a.s.l. Our
26 analysis thus shows that elevation change estimates are in most cases not significantly
27 different if we assume different thresholds for outlier definition or if we consider the
28 uncertainty in our ELA estimate. Significant sensitivity values can be explained by erroneous
29 patterns in the accumulation areas that are properly defined as outliers with a 1σ threshold
30 applied to areas above 5400 m a.s.l.

1 **4.3 Altitudinal distribution of elevation changes**

2 The altitudinal distribution of mean elevation changes clearly show that the thinning patterns
3 of all debris-covered tongues have changed over time (Figure 8, Figure 11). Areas with clear
4 increases in thinning rates can be identified for Langtang Glacier 5000-5150 m a.s.l.
5 (25%-100% thinning rate increase), for Langshisha Glacier 4650-5100 m a.s.l. (25%-260%),
6 for Shalbachum Glacier 4500-4800 m a.s.l. (25%-180%) and for Lirung Glacier 4300-4350
7 m a.s.l. (80%-170%). Thinning rates have remained mostly constant in the lower third of the
8 elevation ranges of the tongues (Langtang, Shalbachum and Lirung Glaciers). At Ghanna
9 Glacier, thinning rates have recently declined near the glacier terminus at 4800-4850 m a.s.l.
10 (60-90% thinning rate decrease, Figure 8e). This pattern of decreasing thinning rates contrasts
11 with all other temporal patterns for debris-covered glacier areas.

12 On Langshisha Glacier (Figure 8b) near the terminus, the comparability of 1974-2006
13 thinning rates with the 2006-2015 ensemble is limited. Here, the glacier tongue became very
14 narrow in the last decade and ultimately a small part below 4500 m a.s.l. disconnected from
15 the main tongue (Figure 1) between 2010 and 2014. The fragmentation of the tongue leads to
16 mean thinning rates close to zero at elevation bands where a substantial part of the glacier
17 area disappears during a given time interval.

18 Overall, the thinning profiles of 2006-2015 ensemble members show very similar
19 characteristics (Figure 8, Figure 11). The profiles diverge for the uppermost elevation bands
20 of the tongues and in the accumulation areas. This agrees with the larger error that is
21 attributed to higher elevations (Figure 3). Above 5500 m a.s.l. it is impossible to separate
22 uncertainty from actual differences in thinning rates.

23 To compare the thinning patterns of debris-covered glaciers to the thinning patterns of debris-
24 free glaciers, the altitudinal distribution of elevation changes at Yala Glacier are presented in
25 Figure 11. Yala Glacier experiences more rapid thinning over almost its entire elevation range
26 in recent periods (Figure 11d). This is in clear contrast to the much less uniform patterns at
27 debris-covered glaciers (Figure 11a-c). Below 5400 m a.s.l there has been a three-fold
28 increase in thinning rates at Yala Glacier, comparing 1974-2006 to the 2006-2015 ensemble
29 results.

30 On Yala Glacier maximal thinning takes place at the terminus and then decreases nearly
31 linearly with altitude until it reaches values close to zero (Figure 11d). For debris-covered
32 glaciers, the elevation corresponding to the maximum thinning rates is different from glacier

1 to glacier. On Shalbachum and Lirung Glaciers the maximum is reached somewhere close to
2 the upper end of the tongue (4650-4750 m a.s.l. and 4300-4400 m a.s.l., respectively, Figure
3 8c and d), on Langtang and Ghanna Glaciers more in the middle part (4950 – 5150 m a.s.l.
4 and 4900-5000 m a.s.l., respectively, Figure 8a and e) and on Langshisha Glacier closer to the
5 terminus (4450-4700 m a.s.l., Figure 8b). On the large debris-covered glaciers, areas of
6 maximum thinning seem to have shifted and extended to higher elevations only at Langtang
7 Glacier, where during the period 1974-2006 maximum thinning occurred between 4850 and
8 4950 m a.s.l. (Figure 8a). On Langtang and Shalbachum Glaciers the difference between
9 thinning near the terminus and maximum thinning became much more pronounced in recent
10 periods, but on Shalbachum Glacier maximum thinning during the period 1974-2006 occurred
11 slightly higher up at 4750 – 4800 m a.s.l. (Figure 8c).

12 Note that the altitudinal $\Delta h/\Delta t$ profiles (Figure 8, Figure 11) always refer to the same position
13 in space, since 50 m elevation bands were delimited only once on the basis of the SRTM
14 1 Arc-Second Global DEM. To account for the up-valley movement of on-glacier elevation
15 bands over time due to surface lowering, profiles would have to be slightly shifted relative to
16 each other. However, given the maximum thinning rates of 1-1.5 ma^{-1} in 1974-2006, the
17 maximum relative adjustment of values in Figure 8 and Figure 11 would never exceed one
18 50 m elevation band. Accounting for the shifting of elevation bands over time would therefore
19 not lead to different conclusions regarding changes in spatial $\Delta h/\Delta t$ patterns.

20 **4.4 Glacier area changes**

21 Debris-free Yala Glacier experienced the strongest increase in relative annual area loss of all
22 studied glaciers (1974-2006: $-0.43 \pm 0.05\% \text{ a}^{-1}$, 2006-2015: $-1.77 \pm 0.16\% \text{ a}^{-1}$, Table 7).
23 During the same two time intervals Kimoshung Glacier shrank only at rates of $0.08 \pm$
24 $0.01\% \text{ a}^{-1}$ and $0.05 \pm 0.02\% \text{ a}^{-1}$, respectively. This represents significantly lower retreat rates
25 for the second period than at Yala Glacier. The differences in area change rates are consistent
26 with the identified differences in mean glacier surface elevation changes, where the two
27 glaciers also represent opposite extremes (Section 4.2).

28 In comparison to the current retreat rates of Yala Glacier, all debris-covered glaciers are
29 shrinking at a much slower pace, with retreat rates between $-0.04 \pm 0.04\% \text{ a}^{-1}$ and $-0.40 \pm$
30 $0.12\% \text{ a}^{-1}$ (Table 7). Also debris-covered glaciers for which we observe high annual volume
31 losses have nearly stationary fronts (e.g. Shalbachum Glacier: 2006-2015 thinning rate $-0.53 \pm$

1 0.19 m a⁻¹, 2006-2015 area loss -0.04 ± 0.04 % a⁻¹). Ghanna Glacier in contrast shows a
2 slightly more significant retreat (-0.40 ± 0.12 % a⁻¹, Table 7), although the mean thinning rates
3 are the least negative of all debris-covered areas (Figure 10).

4 **4.5 Surface velocities and supraglacial cliff/lake areas**

5 Approximately 10% of all grid cells for the three largest debris-covered tongues (Langtang,
6 Langshisha, Shalbachum) contain supraglacial cliff features ('Cliff Area' in Table 8). At
7 Lirung and Ghanna tongues this value decreases to 8% and 3%, respectively. For Ghanna
8 tongue practically no supraglacial lakes could be identified, while at the other debris-covered
9 tongues 'Lake Area' is between 2.3% and 3.3%.

10 The mean surface velocities of the tongues range between 1.6 m a⁻¹ (Ghanna tongue) and 7 m
11 a⁻¹ (Langshisha tongue). The mean and the standard deviation of off-glacier surface velocities
12 are 1.3 m a⁻¹ and 1.9 m a⁻¹, respectively. At Ghanna and Lirung tongue, which both have a
13 mean surface velocity below 3 m a⁻¹, it is therefore practically impossible to discriminate
14 moving ice from quasi-stagnant ice. Following Scherler et al. (2011b), all glacier grid cells
15 with a surface velocity of less than 2.5 m a⁻¹ are therefore termed 'stagnant' for simplicity.
16 According to this definition, the tongue area classified as 'stagnant' (Table 8) ranges from
17 20% (Langshisha tongue) to 85% (Ghanna tongue).

18 In our sample of five debris-covered glaciers, cliffs and lakes seem to appear more frequently
19 on glaciers which are dynamically active. We identify a highly significant negative correlation
20 (Pearson's linear correlation coefficient $r=-0.99$) between cliff area fraction per tongue and the
21 percentage of stagnant tongue area. 'Lake Area' and '% stagnant area' are also negatively
22 correlated ($r=-0.87$). At the scale of individual tongues, a correlation between surface
23 velocities and cliff appearance is evident at Shalbachum Glacier (Figure 12c). Here we
24 identify a correlation of 0.85 (respectively 0.68) between the altitudinal velocity profile and
25 cliff (respectively lake) areas per 50 m elevation band. Also on the two other large debris-
26 covered tongues in the valley, on Langtang and Langshisha tongues, cliff appearance clearly
27 decreases towards the termini where the glaciers are quasi-stagnant (but the highest cliff area
28 densities are identified 200-300 m below the altitude ranges corresponding to maximum
29 surface velocity and therefore the two variables are not linearly correlated).

30 To investigate a possible link between accelerated thinning and the presence of supraglacial
31 lakes and cliffs we compare 'Cliff Area' and 'Lake Area' (as provided in Table 8) to changes

1 in mean thinning rates per tongue ($\Delta \Delta h/\Delta t$, difference between ‘1974-2006’ and ‘ensemble
2 mean 2006-2015’ as provided in Table 5). Overall, the correlation coefficient between
3 fractional cliff area per tongue and $\Delta \Delta h/\Delta t$ is -0.62 (and -0.50 between lake area and
4 $\Delta \Delta h/\Delta t$). The likely reduced thinning rates on Ghanna tongue (Figure 10e) indeed correspond
5 to low cliff and lake area fractions (3.2% and 0.4%, respectively). On Lirung, Shalbachum
6 and Langshisha tongues thinning accelerated by 0.47-0.64 m a^{-1} , whereas fractional cliff and
7 lake areas are similar (cliff area: 8.0-10.5%, lake area: 2.3-2.6%). Also Langtang tongue is
8 characterized by relatively high cliff and lake area fractions (10% and 3.3%, respectively,
9 Table 8) but the identified changes in thinning rates are only minor. The acceleration of mean
10 thinning rates at Langtang tongue is significant at the 95% confidence level (Figure 10a), but
11 the difference in mean thinning rates 1974-2006 and 2006-2015 is only -0.12 m a^{-1} (Table 5).

12 At locations where thinning rates did not increase significantly we mostly identify low cliff
13 area fractions below 10% (e.g. on Langtang tongue below 4750 m a.s.l. and above 5150 m
14 a.s.l., at Shalbachum below 5500 m a.s.l. and at Ghanna tongue). Conversely, cliff area
15 fractions are generally higher than 10% where the 2006-2015 ensemble consistently indicates
16 thinning acceleration (Figure 12). Exception to this observation are the high cliff area
17 fractions at Langtang Glacier 4750-4900 m a.s.l., where thinning rates did not change
18 significantly (Figure 12a), and low cliff area fractions at Shalbachum Glacier 4750-4800 m
19 a.s.l., where thinning rates increased (Figure 12c). Lirung tongue also shows an opposite
20 behavior, except for the lowest elevation band. However, maximum thinning acceleration at
21 4300 m a.s.l. corresponds to a relatively high lake area fraction of 6% (Figure 12d).

22 Altitude bands with no significant increases in thinning rates on Langtang Glacier consistently
23 coincides with relatively low surface velocities below 5 m a^{-1} . At Langshisha and Shalbachum
24 tongues this is also the case (Figure 12). Across all debris-covered glacier tongues, 77% of all
25 elevation bands where thinning accelerated ($\Delta(\Delta h/\Delta t) < -0.2 \text{ m a}^{-1}$) are not stagnating, and in
26 72% of all elevation bands where thinning rates remained constant or declined ($\Delta(\Delta h/\Delta t) \geq$
27 -0.2 m a^{-1}) we observe stagnant conditions with velocities below 2.5 m a^{-1} .

28

1 **5 Discussion**

2 **5.1 Elevation changes of debris-covered glaciers**

3 Elevation changes in the debris-covered area are primarily independent of elevation (Figure
4 8), as previously identified in the Langtang catchment (Pellicciotti et al., 2015) and elsewhere
5 in high-mountain Asia (e.g. Bolch et al., 2011; Dobhal et al., 2013; Pieczonka et al., 2013;
6 Pieczonka and Bolch, 2015; Ye et al., 2015). Such patterns have usually been explained by
7 downglacier increase of debris thickness and by ablation associated with supraglacial lakes
8 and exposed ice cliffs. Our analysis shows that, with few exceptions, the highest thinning
9 rates and the strongest increase in thinning rates can be associated to areas with a high
10 concentration of ice cliffs and supraglacial ponds (Figure 12, Figure S4). While previous
11 studies have pointed out that debris-covered areas with a large presence of supraglacial cliffs
12 and lakes make a disproportionately large contribution to ablation (Reid and Brock, 2014;
13 Buri et al., 2016; Miles et al., 2016a; Thompson et al., 2016), this is the first study which
14 documents the relation between accelerations in volume loss rates and the large presence of
15 supraglacial cliffs and lakes.

16 Accelerated thinning of debris-covered area in the Upper Langtang catchment does not take
17 place on stagnating parts of the tongues, but on the contrary at areas where debris-covered
18 glacier area is dynamically active (Figure 12), and where the transition between the active and
19 the stagnant ice can be expected. Supraglacial cliffs seem to appear more frequently on slowly
20 moving ice ($5\text{-}10\text{ m a}^{-1}$, Figure 12) and not where the glacier is stagnant (Sakai et al., 2002;
21 Bolch et al., 2008; Thompson et al., 2016). This can be explained by compressive stresses
22 associated with flow deceleration that may initiate fracturing (Benn et al., 2009). Such
23 stresses are usually not large enough to initiate open surface crevasses, but in combination
24 with elevated water pressure due to local water inputs lead to hydrologically driven fracture
25 propagation (hydrofracturing) and englacial conduit formation (Benn et al., 2009). The
26 collapse of large englacial voids destabilizes the debris layers and leads to the formation of
27 new ice cliffs.

28 The appearance of supraglacial lakes, on the other hand, is strongly related to the surface
29 gradient (Sakai and Fujita, 2010; Miles et al., 2016b). Large supraglacial lakes can only form
30 where the slope is less than 2° (Reynolds, 2000) and where local water input is high. These
31 conditions are not met on debris-covered glacier sections in the Upper Langtang catchment,

1 since local surface slope is consistently above 5° (Pellicciotti et al., 2015). It is interesting to
2 note that the highest lake area fractions (Lake Area $> 6\%$) are found on avalanche deposition
3 zones at Langtang Glacier (4750-4800 m a.s.l., Figure 9a and Figure 12a) and at Lirung
4 Glacier (4300 m a.s.l., Figure 9d and Figure 12d). This is likely related to high local surface
5 water inputs from melting of avalanche snow and ice. On Langtang Glacier frequent
6 avalanche inputs may explain why thinning did not accelerate at the altitude range between
7 4750 m a.s.l. and 4900 m a.s.l., in spite of the presence of exposed ice (Cliff Area $> 13\%$,
8 Figure 12a).

9 Several studies suggest that lakes and cliffs are important but cannot explain the mass loss
10 alone (e.g. Sakai et al., 2002; Juen et al., 2014). The high thinning magnitudes on the upper
11 sections of Shalbachum tongue (4750-4800 m a.s.l.) likely cannot be attributed to lakes and
12 cliffs (cliff/lake area fractions are below 5%, Figure S4c), and thin layers of deposited debris
13 in the upper sections of the glacier tongue could explain such patterns.

14 Reduced ice fluxes also contribute to thinning accelerations. To assess how much this factor
15 contributes to the observed accelerations in thinning it would be necessary to quantify
16 changes in ice flux over time (e.g. Nuimura et al., 2011; Berthier and Vincent, 2012; Nuth et
17 al., 2012). Information about the evolution of surface velocities over long time periods would
18 be required, which our dataset cannot provide. However, given the usually very slow
19 dynamical response of debris-covered glaciers to changes in the local temperature (Banerjee
20 and Shankar, 2013) it can be assumed that a slowdown of the compressive flow regime is not
21 the primary factor that causes the observed thinning accelerations. Over the timescales
22 considered in this study, on the other hand, high warming rates have been identified in this
23 part of the Himalaya (Shrestha et al., 1999; Lau et al., 2010). The rise in air temperatures
24 directly impacts glacier melt rates, and can explain rapid acceleration of thinning where ice is
25 not insulated from warming by thick debris.

26 Banerjee and Shankar (2013) numerically investigated the response of extensively debris-
27 covered glaciers to rising air-temperatures and describe the dynamical response as follows:
28 during an initial period the fronts remain almost stationary and in the ablation region a slow-
29 flowing quasi-stagnant tongue develops. During this period, which may last more than 100
30 years, glaciers lose volume by thinning. After this initial period glaciers start to retreat with a
31 higher rate, while annual volume loss decreases because of thickening debris layers. Since
32 thinning rates near the fronts of the large debris-covered glaciers in the valley (Langtang,

1 Langshisha and Shalbachum Glaciers) have not yet started to significantly decrease (Figure
2 12a-c) and the glacier tongues are still dynamically active (Figure 13) it can be assumed that
3 the quasi-stationary length period will persist for these glaciers in the near future. The model
4 of Banerjee and Shankar (2013) does not account for supraglacial cliffs and lakes, which
5 likely contribute to thinning acceleration (Figure 12). However, we have shown that they
6 primarily appear on parts of the glacier tongues which are still dynamically active (Table 8). It
7 can thus be assumed that they become less abundant with decreasing flow. The presence of
8 cliffs and lakes therefore does not interfere with the dynamical response of debris-covered
9 glaciers as described by Banerjee and Shankar (2013).

10 Near the snout of Ghanna Glacier a deceleration in thinning rates by -80% can be clearly
11 identified (Figure 8e, 4800-4850 m a.s.l.). Previous studies have provided evidence that
12 ablation rates of debris-covered ice may decrease over time as a consequence of thickening
13 debris cover, in spite of rising air-temperatures (Banerjee and Shankar, 2013; Rowan et al.,
14 2015). This process seems to take place currently at Ghanna tongue, but also on the lower
15 ablation areas of Lirung, Langtang and Shalbachum Glaciers, where the ensemble of thinning
16 rates also point to decreasing rates (Figure 12). The insulating effect of thickening debris
17 might even lead to terminus advance during warmer climatic periods (Kellerer-Pirklbauer et
18 al., 2008). However, terminus advances have not been observed in the study area (Table 8)
19 and are unlikely to occur at the five studied debris-covered glaciers due to ablation from
20 frontal cliffs (evident from higher thinning rates at the lowest elevation bands, Figure 8).

21 **5.1.1 Post-earthquake avalanche impacts**

22 Accumulation by debris-laden avalanches is one of the most important processes for debris-
23 covered glacier formation (Scherler et al., 2011a). The tongue of Lirung Glacier would likely
24 not exist without accumulation through avalanches (Ragettli et al., 2015). It is detached from
25 the accumulation area (Figure 1) and reaches 200-700 m lower elevations than all other
26 debris-covered glaciers (Table 1). Our volume calculations of the post-earthquake avalanche
27 impact allow quantifying the avalanche impact on mass balance and comparing it to mass loss
28 during an average year. Given the avalanche deposits remaining on Lirung tongue by 6 Oct
29 2015 (divided by the area of the tongue: 3.87 ± 0.23 m, Table 4) and the average $\Delta h/\Delta t$ rates
30 between Oct 2006 and Feb 2015 of -1.64 ± 0.10 m a⁻¹ (Figure 10d), the avalanche after the
31 earthquake compensated by 240% the volume loss of one average year. At the scale of all
32 debris-covered area in the valley this value amounts to 50% (0.52 ± 0.19 m avalanche

1 deposits and $1.02 \pm 0.08 \text{ m a}^{-1}$ average thinning). According to Scally and Gardner (1989)
2 avalanche deposit density increases until the end of the ablation season to about 80% of ice
3 density. The mass deposits therefore compensate mass loss during a normal year by about
4 180% at Lirung tongue (40% at the catchment scale). Still, our analysis has revealed that the
5 impacts are not significant in comparison to the 2006-2015 ensemble uncertainty (Section 4.1,
6 Figure 10d and f).

7 **5.2 Elevation changes of debris-free glaciers**

8 2006-2015 downwasting rates on Yala Glacier are $0.5\text{-}1.2 \text{ m a}^{-1}$ higher than on Kimoshung
9 Glacier (Table 5). However, the two glaciers have a very different hypsometry (Figure S5).
10 Currently the estimated AAR of Yala Glacier is 40% (Table 1), which is a common value in
11 the HKH region (Kääb et al., 2012). The estimated AAR of 86% at Kimoshung Glacier, on
12 the other hand, corresponds to an exceptionally high value for the HKH (Khan et al., 2015).
13 The differences in volume loss rates point to the role of glacier hypsometry for the response
14 of debris-free glaciers to climatic changes (e.g. Jiskoot et al., 2009). Almost balanced mass
15 budgets in recent years (Table 5) and only minor area changes (Table 7) are associated to
16 Kimoshung Glacier. Thinning did not increase significantly with respect to the period 1974-
17 2006 (Figure 9g). Due to the steep tongue of this glacier the AAR is also not sensitive to
18 changes in the ELA due to global warming (Table 6), and only a small fraction of area is
19 exposed to rising temperatures above freezing level. The balanced conditions of Kimoshung
20 Glacier therefore indicate that precipitation in recent decades remained approximately stable,
21 which agrees with the findings of studies on precipitation trends in this part of the Himalaya
22 (Shrestha et al., 2000; Immerzeel, 2008; Singh et al., 2008). Yala Glacier, on the other hand,
23 is sensitive to fluctuations in temperature. A hypothetical rise of the ELA by 100 m at this
24 glacier causes 30% of its area to turn from accumulation into ablation area (Table 6), and
25 thinning below the ELA is accelerating rapidly (Figure 11d). Due to the common AAR of
26 Yala Glacier it can be assumed that many other debris-free glaciers in the region are currently
27 thinning at similar rates.

28 **5.3 Differences between debris-free and debris-covered glaciers**

29 The response of debris-covered and debris-free glaciers to warming is substantially different,
30 as described in the two sections above and exemplified by the altitudinal elevation change
31 profiles in Figure 11. Our observations do not support the findings of previous studies about

1 similar present-day lowering rates of debris-covered and debris-free glacier areas at the same
2 elevation (Kääb et al., 2012; Nuimura et al., 2012; Gardelle et al., 2013). Also for debris-
3 covered elevation bands where up to 18% the area is covered by supraglacial cliffs and lakes
4 (e.g. at Langtang tongue 5050 m a.s.l. or at Langshisha tongue 4750 m a.s.l.) thinning rates do
5 not exceed 1.8 m a^{-1} , while for Yala Glacier the lowering rates are already above this value at
6 5250 m a.s.l. and further increase downglacier (Figure 11). Within the same altitudinal range
7 (5200-5300 m a.s.l.) thinning rates of debris-covered glaciers do not exceed 35%-75% of the
8 thinning rates of Yala Glacier.

9 Our data indeed reveal 60%-80% lower thinning rates at Kimoshung tongue with respect to
10 Yala Glacier at 5200-5300 m a.s.l. (Figure S5). Kimoshung Glacier has a very steep tongue
11 that reaches to similarly low elevations as the debris-covered glacier tongues (Table 1).
12 However, a comparison of thinning rates with debris-covered glaciers is not meaningful, since
13 the average slope of Kimoshung tongue is 32%, whereas the average slope of debris-covered
14 area is only 8%. Glacier surface height increase as a result of compressive flow effectively
15 compensates for lowering by ablation on a glacier with a very steep tongue, whereas this is
16 not expected on gently sloped glacier area. We suggest that future large scale geodetic studies
17 take this into account when comparing lowering rates of debris-free and debris-covered ice.

18 Regarding the mean surface elevation changes (Table 5), our observations reveal a
19 heterogeneous response to climate of both the debris-free and the debris-covered glaciers. As
20 discussed in the two sections above, there are examples for both types of glaciers where
21 thinning has increased significantly or where thinning remained approximately constant. A
22 significant difference in thinning trends between debris-free and debris-covered glaciers in
23 our sample cannot be identified. In our sample, the best predictor for thinning accelerations
24 seems to be the altitude distributions of glaciers. Glaciers with a high AAR (Kimoshung) or
25 which reach the highest elevations (Lirung) have the most balanced mass budgets and show
26 no significant changes in volume loss over time (Figure 9, Table 5). Glaciers which are most
27 sensitive to ELA changes (more than $\pm 10\%$ AAR change in response to $\pm 100 \text{ m}$ ELA
28 uncertainty, Table 6) such as Yala, Langtang and Langshisha Glaciers reveal the most
29 significant thinning accelerations (Figure 9, Table 5). However, debris-free Yala Glacier is
30 currently downwasting at 60%-100% higher rates than the large debris-covered glaciers in the
31 valley. Considering Yala Glacier as a benchmark for debris-free glaciers in the Nepal
32 Himalayas (Fujita and Nuimura, 2011), our results indeed point to a difference in current

1 volume loss of debris-free and debris-covered glaciers. It seems important, however, that this
2 observation is confirmed by studies using larger glacier samples.

3 **5.4 Comparison to other studies**

4 The four largest debris-covered glaciers in the valley (Langtang, Langshisha, Shalbachum,
5 Lirung) have been the focus of a recent geodetic mass balance study by Pellicciotti et al.
6 (2015), who reconstructed elevation and mass changes using the 1974 Hexagon DEM which
7 is also used in this study (spatial resolution 30 m) and the 2000 SRTM3 DEM (90 m). They
8 found that all four glaciers lost mass over the study period but with different rates (on average
9 -0.32 ± 0.18 m w.e. a^{-1}). We find an overall glacier mass balance for the period 1974-2006 of
10 the four glaciers which is probably slightly less negative (-0.22 ± 0.08 m w.e. a^{-1}). However,
11 the results match within the uncertainties. A study by Kääb et al. (2015) revealed that the
12 penetration estimate of the SRTM radar signal as applied by Pellicciotti et al. (2015) is likely
13 underestimated. A correction of their results by a larger penetration estimate reconciles their
14 results with ours. The lower uncertainty estimates by our study are justified by the high
15 resolution and quality of the 2006 Cartosat-1 DEM (Table 3). Differences in the mass balance
16 of Langtang, Lirung and Shalbachum Glacier are within uncertainty bounds and can be
17 attributed to differences in used glacier masks, study period, outlier correction approaches and
18 density assumptions. However, for Langshisha Glacier we calculate a mass balance which is
19 substantially less negative than in Pellicciotti et al. (2015). While we identify almost balanced
20 conditions for the period 1974-2006 (-0.10 ± 0.08 m w.e. a^{-1} , Table 5), the mass balance
21 indicated by Pellicciotti et al. (2015) is very negative (-0.79 ± 0.18 m w.e. a^{-1}). The
22 discrepancy can be explained by the overestimated extent of the accumulation areas by
23 Pellicciotti et al. (2015) (Figure S2) in combination with unrealistic lowering rates of up to
24 -2 m a^{-1} at about 6000 m a.s.l. (Figure 4d in Pellicciotti et al., 2015). The more realistic
25 elevation change values obtained by the present study for the accumulation areas (-0.4 - 0.4
26 m a^{-1} , Figure 11b) point to the need of restrictive outlier definitions and the advantage of
27 having information from multiple datasets available for gap filling.

28 Yala Glacier has been frequently visited for field measurements in the last 25 years.
29 Sugiyama et al. (2013) calculated mean thinning rates of Yala Glacier for the periods 1982-
30 1996 (-0.69 ± 0.25 m a^{-1}) and 1996-2009 (-0.75 ± 0.24 m a^{-1}) on the basis of ground
31 photogrammetry and GPS surveys. The values suggest a more moderate acceleration of
32 volume loss rates than in our study (-0.33 ± 0.06 m a^{-1} 1974-2006 to -0.89 ± 0.23 m a^{-1} 2006-

1 2015, Table 5). However, similarly to our study Sugiyama et al. (2013) identified a rapid
2 acceleration of thinning rates at the lowest elevations. At higher elevations the uncertainty of
3 photogrammetric surveys increases because of low contrast due to homogeneous snow layers.
4 Ragettli et al. (2015) used a glacio-hydrological model to calculate the mass balances of all
5 glaciers in the upper Langtang catchment for the hydrological year 2012/2013. They used
6 glaciological and meteorological field data from Lirung and Yala Glacier to calibrate the melt
7 parameters taking into account the effect of variable debris thickness and spatio-temporal
8 changes in surface albedo. The calculated average mass balance of glaciers in the valley was
9 -0.24 m w.e. Here we identify mass balances which were substantially more negative during
10 recent periods (-0.45 ± 0.18 m w.e. a^{-1} , Table 5). However, the hydrological year 2012/2013
11 was one of the wettest years since 1990 (Ragettli et al., 2015), which likely explains the less
12 negative mass balances.

13 The acceleration in mass loss in recent periods identified by this study agrees with other
14 studies from the Nepalese Himalaya which assess multi-temporal elevation changes (Bolch et
15 al., 2011; Nuimura et al., 2012). Bolch et al. (2011) identify an increase in mass loss rates by
16 0.47 m w.e. a^{-1} comparing the two periods 1970-2007 (-0.32 ± 0.08 m w.e. a^{-1}) and 2002-2007
17 (-0.79 ± 0.52 m w.e. a^{-1}). Nuimura et al. (2012) calculate increasing mass losses in the same
18 study region between 1992-2008 (-0.26 ± 0.24 m w.e. a^{-1}) and 2000-2008 (-0.45 ± 0.60 m
19 w.e. a^{-1}). However, the identified acceleration in glacier thinning is not significant given the
20 largely overlapping error bounds. Moreover, the mass loss estimates of Gardelle et al. (2013)
21 for the Khumbu region and the period 2001-2011 (average of -0.41 ± 0.21 m w.e. a^{-1}) are in
22 the same order as calculated by Bolch et al. (2011) for 1970-2007. The ensemble approach of
23 this study can therefore substantially strengthen previous conclusions that mass loss of
24 glaciers in the Central Himalaya is accelerating. The volume changes calculated over several
25 multi-year periods between 2006 and 2015 consistently indicate that glacier thinning has
26 indeed accelerated (Figure 9h).

27

28 **6 Conclusions**

29 This study presents glacier volume changes of seven glaciers (five partially debris-covered,
30 two debris-free) in the upper Langtang catchment in Nepal, using a digital elevation model
31 (DEM) from 1974 stereo Hexagon satellite data and seven DEMs derived from 2006-2015
32 stereo or tri-stereo satellite imagery. We carefully selected elevation change maps which are

1 least affected by uncertainty to obtain multiple independent DEM differences for the period
2 2006-2015.

3 Our results point to increasing thinning rates, from $-0.24 \pm 0.08 \text{ m a}^{-1}$ in 1974-2006 to $-0.45 \pm$
4 0.18 m a^{-1} in 2006-2015, where the estimated confidence level of accelerated thinning rates is
5 higher than 99%. This study therefore supports the findings of previous studies (Bolch et al.,
6 2011; Nuimura et al., 2012) that glacier wastage in the Central Himalaya is accelerating.
7 However, whereas a majority of glaciers in the study region are thinning rapidly, glaciers with
8 a high accumulation area have almost balanced mass budgets and experience no or only
9 insignificant accelerations in thinning.

10 Our observations also reveal that thinning has mostly accelerated in the upper reaches of the
11 tongues (up to +150%, comparing the periods 1974-2006 and 2006-2015), while the nearly
12 stagnant areas near the terminus show constant or decreasing thinning rates (up to -80%). The
13 quality of the elevation change information is high due to good image contrast over debris,
14 which increases the accuracy of the geodetically derived DEMs. The variations in the
15 elevation change profiles of debris-covered tongues are mostly within $\pm 10\%$, in the six
16 overlapping periods between 2006 and 2015. The highest thinning rates and the strongest
17 increase in thinning rates can be associated to areas with a high concentration of ice cliffs and
18 supraglacial ponds. Constant or decelerating thinning rates can be associated to areas with
19 relatively homogeneous debris layers near the termini of glaciers. We conclude that the
20 response of extensively debris-covered glaciers to global warming is largely determined by
21 feedback processes associated to different surface characteristics.

22 The behavior of glaciers in the study area is highly heterogeneous, and the presence of debris
23 itself is not a good predictor for mass balance trends. However, the spatial thinning patterns
24 on debris-covered glaciers are fundamentally different than those on debris-free glaciers.
25 While on debris-free glaciers thinning rates are linearly dependent on elevation, debris-
26 covered glaciers have highly non-linear altitudinal elevation change profiles. Our
27 observations do not provide evidence for the existence of a so-called debris-cover anomaly,
28 where the insulating effect of thick supraglacial debris is compensated by enhanced melt from
29 exposed ice cliffs or due to high energy absorption at supraglacial ponds. Within the same
30 altitudinal range, lowering rates on debris-free Yala Glacier are 35%-300% higher than on
31 debris-covered glacier area. On debris-free Kimoshung Glacier the thinning rates are similar
32 to those of debris-covered area, but this result must be explained by compressive flows that

1 compensate for surface lowering by ablation, since the glacier has a very short and steep
2 tongue and a large accumulation area.

3 Geodetic mass balance studies such as this have been increasingly revealing heterogeneous
4 patterns of changes and a complex response of debris-covered glaciers that call for an
5 enhanced understanding of processes over debris-covered glaciers. Their ablation, mass
6 balance and response to climate is modulated by debris supply, transport, glacier flow, lakes
7 and cliffs developments and a complex subglacial hydrology and hydraulics that all need to be
8 understood in the future to be able to predict future changes of these glaciers over multiple
9 time scales.

10 **Acknowledgements**

11 This study is funded by the Swiss National Science Foundation (SNF) project UNCOMUN
12 (Understanding Contrasts in High Mountain Hydrology in Asia). T. Bolch acknowledges
13 funding through German Research Foundation (DFG, code BO 3199/2-1) and European
14 Space Agency (Glaciers_cci project, code 400010177810IAM). We thank Evan Miles for
15 helping with the glacier delineations and the post-processing of surface velocity data. Jakob
16 Steiner and Pascal Buri manually delineated cliffs and lakes for the inventories used in this
17 study, and they are gratefully acknowledged. We thank Etienne Berthier for the Pléiades
18 image data, for his useful comments regarding the DEM extraction and Fanny Brun for her
19 help with the identification of GCPs. DigitalGlobe imagery was used to produce the
20 WorldView-1 and 2 digital elevation models. We thank Eyjolfur Magnússon and one
21 anonymous reviewer for extensive and thorough reviews that considerably helped to improve
22 the manuscript.

23

1 **References**

- 2 Banerjee, A. and Shankar, R.: On the response of Himalayan glaciers to climate change, *J.*
3 *Glaciol.*, 59(215), 480–490, doi:10.3189/2013JoG12J130, 2013.
- 4 Benn, D., Gulley, J., Luckman, A., Adamek, A. and Glowacki, P. S.: Englacial drainage
5 systems formed by hydrologically driven crevasse propagation, *J. Glaciol.*, 55(191), 513–523,
6 doi:10.3189/002214309788816669, 2009.
- 7 Berthier, E. and Vincent, C.: Relative contribution of surface mass-balance and ice-flux
8 changes to the accelerated thinning of Mer de Glace, French Alps, over 1979–2008, *J.*
9 *Glaciol.*, 58(209), 501–512, doi:10.3189/2012JoG11J083, 2012.
- 10 Berthier, E., Arnaud, Y., Kumar, R., Ahmad, S., Wagnon, P. and Chevallier, P.: Remote
11 sensing estimates of glacier mass balances in the Himachal Pradesh (Western Himalaya,
12 India), *Remote Sens. Environ.*, 108(3), 327–338, doi:10.1016/j.rse.2006.11.017, 2007.
- 13 Berthier, E., Vincent, C., Magnússon, E., Gunnlaugsson, Á. Þ., Pitte, P., Le Meur, E.,
14 Masiokas, M., Ruiz, L., Pálsson, F., Belart, J. M. C. and Wagnon, P.: Glacier topography and
15 elevation changes derived from Pléiades sub-meter stereo images, *Cryosph.*, 8(6), 2275–2291,
16 doi:10.5194/tc-8-2275-2014, 2014.
- 17 Bignone, F. and Umakawa, H.: Assessment of ALOS PRISM digital elevation model
18 extraction over Japan, *Int. Arch. Photogramm. Remote Sens. Spat. Inf. Sci.*, 37, 1135–1138,
19 2008.
- 20 Bolch, T., Buchroithner, M. and Pieczonka, T.: Planimetric and volumetric glacier changes in
21 the Khumbu Himal, Nepal, since 1962 using Corona, Landsat TM and ASTER data, *J.*
22 *Glaciol.*, 54(187), 592–600, doi:10.3189/002214308786570782, 2008.
- 23 Bolch, T., Pieczonka, T. and Benn, D. I.: Multi-decadal mass loss of glaciers in the Everest
24 area (Nepal Himalaya) derived from stereo imagery, *Cryosph.*, 5(2), 349–358, doi:10.5194/tc-
25 5-349-2011, 2011.
- 26 Bolch, T., Kulkarni, A., Käab, A., Huggel, C., Paul, F., Cogley, J. G., Frey, H., Kargel, J. S.,
27 Fujita, K., Scheel, M., Bajracharya, S. and Stoffel, M.: The state and fate of Himalayan
28 glaciers., *Science*, 336(6079), 310–314, doi:10.1126/science.1215828, 2012.
- 29 Brun, F., Buri, P., Miles, E. S., Wagnon, P., Steiner, J., Berthier, E., Ragettli, S., Immerzeel,
30 W. W. and Pellicciotti, F.: Quantifying volume loss from ice cliffs on debris-covered glaciers
31 using high resolution terrestrial and aerial photogrammetry, *J. Glaciol.*, 1–12,
32 doi:10.1017/jog.2016.54, 2016.
- 33 Buri, P., Pellicciotti, F., Steiner, J. F., Miles, E. S. and Immerzeel, W. W.: A grid-based model
34 of backwasting of supraglacial ice cliffs on debris-covered glaciers, *Ann. Glaciol.*, 57(71),
35 199–211, doi:10.3189/2016AoG71A059, 2016.

- 1 Burnett, M.: Hexagon (KH-9) Mapping Program and Evolution, National Reconnaissance
2 Office, Chantilly, Virginia., 2012.
- 3 Collier, E. and Immerzeel, W.: High-resolution modeling of atmospheric dynamics in the
4 Nepalese Himalaya, *J. Geophys. Res. Atmos.*, 120, 9882–9896,
5 doi:10.1002/2015JD023266.Received, 2015.
- 6 Dehecq, A., Gourmelen, N. and Trouve, E.: Deriving large-scale glacier velocities from a
7 complete satellite archive: Application to the Pamir–Karakoram–Himalaya, *Remote Sens.*
8 *Environ.*, 162, 55–66, doi:10.1016/j.rse.2015.01.031, 2015.
- 9 Dobhal, D. P., Mehta, M. and Srivastava, D.: Influence of debris cover on terminus retreat
10 and mass changes of Chorabari Glacier, Garhwal region, central Himalaya, India, *J. Glaciol.*,
11 59(217), 961–971, doi:10.3189/2013JoG12J180, 2013.
- 12 Fujita, K.: Effect of precipitation seasonality on climatic sensitivity of glacier mass balance,
13 *Earth Planet. Sci. Lett.*, 276(1-2), 14–19, doi:10.1016/j.epsl.2008.08.028, 2008.
- 14 Fujita, K. and Nuimura, T.: Spatially heterogeneous wastage of Himalayan glaciers., *Proc.*
15 *Natl. Acad. Sci. U. S. A.*, 108(34), 14011–14014, doi:10.1073/pnas.1106242108, 2011.
- 16 Gardelle, J., Berthier, E., Arnaud, Y. and Kääb, a.: Region-wide glacier mass balances over
17 the Pamir-Karakoram-Himalaya during 1999–2011, *Cryosph.*, 7(4), 1263–1286,
18 doi:10.5194/tc-7-1263-2013, 2013.
- 19 Holzer, N., Vijay, S., Yao, T., Xu, B., Buchroithner, M. and Bolch, T.: Four decades of
20 glacier variations at Muztagh Ata (eastern Pamir): a multi-sensor study including Hexagon
21 KH-9 and Pléiades data, *Cryosph.*, 9(6), 2071–2088, doi:10.5194/tc-9-2071-2015, 2015.
- 22 Huss, M.: Density assumptions for converting geodetic glacier volume change to mass
23 change, *Cryosph.*, 7(3), 877–887, doi:10.5194/tc-7-877-2013, 2013.
- 24 Huss, M., Jouvett, G., Farinotti, D. and Bauder, A.: Future high-mountain hydrology: a new
25 parameterization of glacier retreat, *Hydrol. Earth Syst. Sci.*, 14(5), 815–829,
26 doi:10.5194/hess-14-815-2010, 2010.
- 27 Immerzeel, W.: Historical trends and future predictions of climate variability in the
28 Brahmaputra basin, *Int. J. Climatol.*, 28(2), 243–254, doi:10.1002/joc.1528, 2008.
- 29 Immerzeel, W. W., Kraaijenbrink, P. D. a., Shea, J. M., Shrestha, A. B., Pellicciotti, F.,
30 Bierkens, M. F. P. and de Jong, S. M.: High-resolution monitoring of Himalayan glacier
31 dynamics using unmanned aerial vehicles, *Remote Sens. Environ.*, 150, 93–103,
32 doi:10.1016/j.rse.2014.04.025, 2014a.
- 33 Immerzeel, W. W., Petersen, L., Ragettli, S. and Pellicciotti, F.: The importance of observed
34 gradients of air temperature and precipitation for modeling runoff from a glacierized
35 watershed in the Nepalese Himalayas, *Water Resour. Res.*, 50(3), 2212–2226,
36 doi:10.1002/2013WR014506, 2014b.

- 1 Jiskoot, H., Curran, C. J., Tessler, D. L. and Shenton, L. R.: Changes in Clemenceau Icefield
2 and Chaba Group glaciers, Canada, related to hypsometry, tributary detachment, length–slope
3 and area–aspect relations, *Ann. Glaciol.*, 50(53), 133–143,
4 doi:10.3189/172756410790595796, 2009.
- 5 Juen, M., Mayer, C., Lambrecht, a., Han, H. and Liu, S.: Impact of varying debris cover
6 thickness on ablation: a case study for Koxkar Glacier in the Tien Shan, *Cryosph.*, 8(2), 377–
7 386, doi:10.5194/tc-8-377-2014, 2014.
- 8 Kääh, A., Berthier, E., Nuth, C., Gardelle, J. and Arnaud, Y.: Contrasting patterns of early
9 twenty-first-century glacier mass change in the Himalayas, *Nature*, 488(7412), 495–498,
10 doi:10.1038/nature11324, 2012.
- 11 Kääh, A., Treichler, D., Nuth, C. and Berthier, E.: Brief Communication: Contending
12 estimates of 2003–2008 glacier mass balance over the Pamir–Karakoram–Himalaya,
13 *Cryosph.*, 9(2), 557–564, doi:10.5194/tc-9-557-2015, 2015.
- 14 Kargel, J., Leonard, G., Shugar, D., et al.: Geomorphic and geologic controls of geohazards
15 induced by Nepal’s 2015 Gorkha earthquake, *Science*, 351(6269), 1–18,
16 doi:10.1126/science.aac8353, 2016.
- 17 Kellerer-Pirklbauer, A., Lieb, G., Avian, M. and Gspurning, J.: The response of partially
18 debris-covered valley glaciers to climate change: the example of the Pasterze Glacier
19 (Austria) in the period 1964 to 2006, *Geogr. Ann. Ser. A Phys. Geogr.*, 90(4), 269–285,
20 doi:10.1111/j.1468-0459.2008.00345.x, 2008.
- 21 Khan, A., Naz, B. S. and Bowling, L. C.: Separating snow, clean and debris covered ice in the
22 Upper Indus Basin, Hindukush-Karakoram-Himalayas, using Landsat images between 1998
23 and 2002, *J. Hydrol.*, 521, 46–64, doi:10.1016/j.jhydrol.2014.11.048, 2015.
- 24 Lamsal, D., Sawagaki, T. and Watanabe, T.: Digital terrain modelling using Corona and
25 ALOS PRISM data to investigate the distal part of Imja Glacier, Khumbu Himal, Nepal, *J.*
26 *Mt. Sci.*, 8(3), 390–402, doi:10.1007/s11629-011-2064-0, 2011.
- 27 Lau, W. K. M., Kim, M.-K., Kim, K.-M. and Lee, W.-S.: Enhanced surface warming and
28 accelerated snow melt in the Himalayas and Tibetan Plateau induced by absorbing aerosols,
29 *Environ. Res. Lett.*, 5(2), 025204, doi:10.1088/1748-9326/5/2/025204, 2010.
- 30 Leprince, S., Barbot, S., Ayoub, F. and Avouac, J.-P.: Automatic and precise
31 orthorectification, coregistration, and subpixel correlation of satellite images, application to
32 ground deformation measurements, *IEEE Trans. Geosci. Remote Sens.*, 45(6), 1529–1558,
33 2007.
- 34 Magnússon, E., Muñoz-Cobo Belart, J., Pálsson, F., Ágústsson, H. and Crochet, P.: Geodetic
35 mass balance record with rigorous uncertainty estimates deduced from aerial photographs and
36 lidar data – Case study from Drangajökull ice cap, NW Iceland, *Cryosph.*, 10(1), 159–177,
37 doi:10.5194/tc-10-159-2016, 2016.

- 1 Mattson, L. E., Gardner, J. S. and Young, G. J.: Ablation on Debris Covered Glaciers: an
2 Example from the Rakhiot Glacier, Punjab, Himalaya, IAHS Publ., 218, 289–296, 1993.
- 3 Maurer, J. and Rupper, S.: Tapping into the Hexagon spy imagery database: A new automated
4 pipeline for geomorphic change detection, ISPRS J. Photogramm. Remote Sens., 108, 113–
5 127, doi:10.1016/j.isprsjprs.2015.06.008, 2015.
- 6 Mayer, C., Lambrecht, A., Belo, M., Smiraglia, C. and Diolaiuti, G.: Glaciological
7 characteristics of the ablation zone of Baltoro glacier, Karakoram, Pakistan, Ann. Glaciol.,
8 43(1), 123–131, doi:10.3189/172756406781812087, 2006.
- 9 Mihalcea, C., Mayer, C., Diolaiuti, G., Lambrecht, A., Smiraglia, C. and Tartari, G.: Ice
10 ablation and meteorological conditions on the debris-covered area of Baltoro glacier,
11 Karakoram, Pakistan, Ann. Glaciol., 43(1), 292–300, doi:10.3189/172756406781812104,
12 2006.
- 13 Mihalcea, C., Mayer, C., Diolaiuti, G., Agata, C. D., Smiraglia, C., Lambrecht, A.,
14 Vuillermoz, E. and Tartari, G.: Spatial distribution of debris thickness and melting from
15 remote-sensing and meteorological data, at debris-covered Baltoro glacier, Karakoram,
16 Pakistan, Ann. Glaciol., 48(1), 49–57, doi:10.3189/172756408784700680, 2008.
- 17 Miles, E. S., Pellicciotti, F., Willis, I. C., Steiner, J. F., Buri, P. and Arnold, N. S.: Refined
18 energy-balance modelling of a supraglacial pond, Langtang Khola, Nepal, Ann. Glaciol.,
19 57(71), 29–40, doi:10.3189/2016AoG71A421, 2016a.
- 20 Miles, E. S., Willis, I. C., Arnold, N. S. and Pellicciotti, F.: Spatial, seasonal, and interannual
21 variability of supraglacial ponds in the Langtang Valley of Nepal, 1999 to 2013, J. Glaciol.,
22 under revision, 2016b.
- 23 Noh, M.-J. and Howat, I. M.: Automated stereo-photogrammetric DEM generation at high
24 latitudes: Surface Extraction with TIN-based Search-space Minimization (SETSM) validation
25 and demonstration over glaciated regions, GIScience Remote Sens., 52(2), 198–217,
26 doi:10.1080/15481603.2015.1008621, 2015.
- 27 Nuimura, T., Fujita, K., Fukui, K., Asahi, K., Aryal, R. and Ageta, Y.: Temporal Changes in
28 Elevation of the Debris-Covered Ablation Area of Khumbu Glacier in the Nepal Himalaya
29 since 1978, Arctic, Antarct. Alp. Res., 43(2), 246–255, doi:10.1657/1938-4246-43.2.246,
30 2011.
- 31 Nuimura, T., Fujita, K., Yamaguchi, S. and Sharma, R. R.: Elevation changes of glaciers
32 revealed by multitemporal digital elevation models calibrated by GPS survey in the Khumbu
33 region, Nepal Himalaya, 1992–2008, J. Glaciol., 58(210), 648–656,
34 doi:10.3189/2012JoG11J061, 2012.
- 35 Nuimura, T., Sakai, A., Taniguchi, K., Nagai, H., Lamsal, D., Tsutaki, S., Kozawa, A.,
36 Hoshina, Y., Takenaka, S., Omiya, S., Tsunematsu, K., Tshering, P. and Fujita, K.: The
37 GAMDAM glacier inventory: a quality-controlled inventory of Asian glaciers, Cryosph., 9(3),
38 849–864, doi:10.5194/tc-9-849-2015, 2015.

- 1 Nuth, C. and Kääb, A.: Co-registration and bias corrections of satellite elevation data sets for
2 quantifying glacier thickness change, *Cryosph.*, 5(1), 271–290, doi:10.5194/tc-5-271-2011,
3 2011.
- 4 Nuth, C., Schuler, T. V., Kohler, J., Altena, B. and Hagen, J. O.: Estimating the long-term
5 calving flux of Kronebreen, Svalbard, from geodetic elevation changes and mass-balance
6 modelling, *J. Glaciol.*, 58(207), 119–133, doi:10.3189/2012JoG11J036, 2012.
- 7 Östrem, G.: Ice melting under a thin layer of moraine, and the existence of ice cores in
8 moraine ridges, *Geogr. Ann.*, 41(4), 228–230, 1959.
- 9 Paul, F., Barrand, N. E., Baumann, S., Berthier, E., Bolch, T., Casey, K., Frey, H., Joshi, S.
10 P., Konovalov, V., Bris, R. Le, Mölg, N., Nosenko, G., Nuth, C., Pope, a., Racoviteanu, a.,
11 Rastner, P., Raup, B., Scharrer, K., Steffen, S. and Winsvold, S.: On the accuracy of glacier
12 outlines derived from remote-sensing data, *Ann. Glaciol.*, 54(63), 171–182,
13 doi:10.3189/2013AoG63A296, 2013.
- 14 Pellicciotti, F., Stephan, C., Miles, E., Immerzeel, W. W. and Bolch, T.: Mass-balance
15 changes of the debris-covered glaciers in the Langtang Himal, Nepal, 1974–99, *J. Glaciol.*,
16 61(225), doi:10.3189/2015JoG13J237, 2015.
- 17 Pieczonka, T. and Bolch, T.: Region-wide glacier mass budgets and area changes for the
18 Central Tien Shan between ~1975 and 1999 using Hexagon KH-9 imagery, *Glob. Planet.*
19 *Change*, 128, 1–13, doi:10.1016/j.gloplacha.2014.11.014, 2015.
- 20 Pieczonka, T., Bolch, T. and Buchroithner, M.: Generation and evaluation of multitemporal
21 digital terrain models of the Mt. Everest area from different optical sensors, *ISPRS J.*
22 *Photogramm. Remote Sens.*, 66(6), 927–940, doi:10.1016/j.isprsjprs.2011.07.003, 2011.
- 23 Pieczonka, T., Bolch, T., Junfeng, W. and Shiyin, L.: Heterogeneous mass loss of glaciers in
24 the Aksu-Tarim Catchment (Central Tien Shan) revealed by 1976 KH-9 Hexagon and 2009
25 SPOT-5 stereo imagery, *Remote Sens. Environ.*, 130, 233–244,
26 doi:10.1016/j.rse.2012.11.020, 2013.
- 27 Pratap, B., Dobhal, D. P., Mehta, M. and Bhambri, R.: Influence of debris cover and altitude
28 on glacier surface melting: a case study on Dokriani Glacier, central Himalaya, India, *Ann.*
29 *Glaciol.*, 56(70), 9–16, doi:10.3189/2015AoG70A971, 2015.
- 30 Racoviteanu, A. E., Arnaud, Y., Williams, M. W. and Manley, W. F.: Spatial patterns in
31 glacier characteristics and area changes from 1962 to 2006 in the Kanchenjunga–Sikkim area,
32 eastern Himalaya, *Cryosph.*, 9(2), 505–523, doi:10.5194/tc-9-505-2015, 2015.
- 33 Ragettli, S., Pellicciotti, F., Immerzeel, W. W., Miles, E. S., Petersen, L., Heynen, M., Shea,
34 J. M., Stumm, D., Joshi, S. and Shrestha, A.: Unraveling the hydrology of a Himalayan
35 catchment through integration of high resolution in situ data and remote sensing with an
36 advanced simulation model, *Adv. Water Resour.*, 78, 94–111,
37 doi:10.1016/j.advwatres.2015.01.013, 2015.

- 1 Reid, T. D. and Brock, B. W.: Assessing ice-cliff backwasting and its contribution to total
2 ablation of debris-covered Miage glacier, Mont Blanc massif, Italy, *J. Glaciol.*, 60(219), 3–13,
3 doi:10.3189/2014JoG13J045, 2014.
- 4 Reynolds, J.: On the formation of supraglacial lakes on debris-covered glaciers, *IAHS Publ.*,
5 (264), 153–161, 2000.
- 6 Rowan, A. V., Egholm, D. L., Quincey, D. J. and Glasser, N. F.: Modelling the feedbacks
7 between mass balance, ice flow and debris transport to predict the response to climate change
8 of debris-covered glaciers in the Himalaya, *Earth Planet. Sci. Lett.*, 430, 427–438,
9 doi:10.1016/j.epsl.2015.09.004, 2015.
- 10 Sakai, A. and Fujita, K.: Formation conditions of supraglacial lakes on debris-covered
11 glaciers in the Himalaya, *J. Glaciol.*, 56(195), 177–181, doi:10.3189/002214310791190785,
12 2010.
- 13 Sakai, A., Nakawo, M. and Fujita, K.: Melt rate of ice cliffs on the Lirung Glacier, Nepal
14 Himalayas, 1996, *Bull. Glacier Res.*, 16, 57–66, 1998.
- 15 Sakai, A., Takeuchi, N., Fujita, K. and Nakawo, M.: Role of supraglacial ponds in the
16 ablation process of a debris-covered glacier in the Nepal Himalayas, *Debris-Covered Glaciers*,
17 *IAHS Publ.*, 265, 119–130, 2000.
- 18 Sakai, A., Nakawo, M. and Fujita, K.: Distribution characteristics and energy balance of ice
19 cliffs on debris-covered glaciers, Nepal Himalaya, *Arctic, Antarct. Alp. Res.*, 34(1), 12–19,
20 doi:10.2307/1552503, 2002.
- 21 Sapiano, J., Harrison, W. and Echelmeyer, K.: Elevation, volume and terminus changes of
22 nine glaciers in North America, *J. Glaciol.*, 44(146), 119–135, doi:10.3198/1998JoG44-146-
23 119-135, 1998.
- 24 Scally, F. De and Gardner, J.: Evaluation of avalanche mass determination approaches: an
25 example from the Himalaya, Pakistan, *J. Glaciol.*, 35(120), 248–252, 1989.
- 26 Scherler, D., Leprince, S. and Strecker, M.: Glacier-surface velocities in alpine terrain from
27 optical satellite imagery—Accuracy improvement and quality assessment, *Remote Sens.*
28 *Environ.*, 112(10), 3806–3819, doi:10.1016/j.rse.2008.05.018, 2008.
- 29 Scherler, D., Bookhagen, B. and Strecker, M. R.: Hillslope-glacier coupling: The interplay of
30 topography and glacial dynamics in High Asia, *J. Geophys. Res.*, 116(F02019), 1–21,
31 doi:10.1029/2010JF001751, 2011a.
- 32 Scherler, D., Bookhagen, B. and Strecker, M. R.: Spatially variable response of Himalayan
33 glaciers to climate change affected by debris cover, *Nat. Geosci.*, 4(3), 156–159,
34 doi:10.1038/ngeo1068, 2011b.
- 35 Schwitter, M. and Raymond, C.: Changes in the longitudinal profiles of glaciers during
36 advance and retreat, *J. Glaciol.*, 39(133), 582–590, 1993.

- 1 Shrestha, A., Wake, C., Mayewski, P. and Dibb, J.: Maximum temperature trends in the
2 Himalaya and its vicinity: An analysis based on temperature records from Nepal for the
3 period 1971-94, *J. Clim.*, 12, 2775–2786, doi:10.1175/1520-
4 0442(1999)012<2775:MTTITH>2.0.CO;2, 1999.
- 5 Shrestha, A., Wake, C., Dibb, J. and Mayewski, P.: Precipitation fluctuations in the Nepal
6 Himalaya and its vicinity and relationship with some large scale climatological parameters,
7 *Int. J. Climatol.*, 20(3), 317–327, doi:10.1002/(SICI)1097-0088(20000315)20:3<317::AID-
8 JOC476>3.0.CO;2-G, 2000.
- 9 Singh, P., Kumar, V., Thomas, T. and Arora, M.: Changes in rainfall and relative humidity in
10 river basins in northwest and central India, *Hydrol. Process.*, 22(16), 2982–2992,
11 doi:10.1002/hyp.6871, 2008.
- 12 Steiner, J. F., Pellicciotti, F., Buri, P., Miles, E. S., Immerzeel, W. W. and Reid, T. D.:
13 Modelling ice-cliff backwasting on a debris-covered glacier in the Nepalese Himalaya, *J.*
14 *Glaciol.*, 61(229), 889–907, doi:10.3189/2015JoG14J194, 2015.
- 15 Steiner, J. F., Buri, P., Miles, E. S., Ragettli, S. and Pellicciotti, F.: Life and death of ice cliffs
16 and lakes on debris covered glaciers - insights from a new dataset, *Geophys. Res. Abstr.*,
17 18(EGU2016-13922), 2016.
- 18 Sugiyama, S., Fukui, K., Fujita, K., Tone, K. and Yamaguchi, S.: Changes in ice thickness
19 and flow velocity of Yala Glacier, Langtang Himal, Nepal, from 1982 to 2009, *Ann. Glaciol.*,
20 54(64), 157–162, doi:10.3189/2013AoG64A111, 2013.
- 21 Surazakov, A. and Aizen, V.: Positional Accuracy Evaluation of Declassified Hexagon KH-9
22 Mapping Camera Imagery, *Photogramm. Eng. Remote Sens.*, 76(5), 603–608,
23 doi:10.14358/PERS.76.5.603, 2010.
- 24 Tadono, T. and Shimada, M.: Calibration of PRISM and AVNIR-2 onboard ALOS “Daichi,”
25 *IEEE Trans. Geosci. Remote Sens. Sens.*, 47(12), 4042–4050,
26 doi:10.1109/TGRS.2009.2025270, 2009.
- 27 Thompson, S., Benn, D. I., Mertes, J. and Luckman, A.: Stagnation and mass loss on a
28 Himalayan debris-covered glacier: processes, patterns and rates, *J. Glaciol.*, 1–19,
29 doi:10.1017/jog.2016.37, 2016.
- 30 Tiwari, P., Pande, H., Punia, M. and Dadhwal, V. K.: Cartosat-I: Evaluating mapping
31 capabilities, *Int. J. Geoinformatics*, 4(1), 51–56 [online] Available from:
32 <http://creativitycity.gssc.osaka-cu.ac.jp/IJG/article/view/609> (Accessed 26 January 2016),
33 2008.
- 34 Wang, D. and Käab, A.: Modeling Glacier Elevation Change from DEM Time Series, *Remote*
35 *Sens.*, 7(8), 10117–10142, doi:10.3390/rs70810117, 2015.
- 36 Yao, T., Thompson, L., Yang, W., Yu, W., Gao, Y., Guo, X., Yang, X., Duan, K., Zhao, H.,
37 Xu, B., Pu, J., Lu, A., Xiang, Y., Kattel, D. B. and Joswiak, D.: Different glacier status with

1 atmospheric circulations in Tibetan Plateau and surroundings, *Nat. Clim. Chang.*, 2(9), 663–
2 667, doi:10.1038/nclimate1580, 2012.

3 Ye, Q., Bolch, T., Naruse, R., Wang, Y., Zong, J., Wang, Z., Zhao, R., Yang, D. and Kang,
4 S.: Glacier mass changes in Rongbuk catchment on Mt. Qomolangma from 1974 to 2006
5 based on topographic maps and ALOS PRISM data, *J. Hydrol.*, 530, 273–280,
6 doi:10.1016/j.jhydrol.2015.09.014, 2015.

7

1 Figures and Tables

2 Table 1. Characteristics of the studied glaciers in the upper Langtang catchment. The
 3 measures are based on the SRTM 1 Arc-Second Global DEM and glacier outlines of 2006.

Name	Area km ²	Debris cover km ²	Mean slope %	Mean slope glacier tongue* %	AAR**	Elevation range m a.s.l.
1 Langtang	46.5	15.5	17.1	7.2	52%	4479-6615
2 Langshisha	16.3	4.5	17.7	7.5	55%	4415-6771
3 Shalbachum	10.2	2.6	16.9	9.1	52%	4231-6458
4 Lirung	6.5	1.1	34.0	9.9	49%	4044-7120
5 Ghanna	1.4	0.7	20.9	15.5	15%	4721-5881
6 Kimoshung	4.4	-	24.4	32.1	86%	4385-6648
7 Yala	1.9	-	22.7	20.3	40%	5122-5676

*Here we consider the debris-covered area for glaciers with debris-covered tongues and all glacier area below 5400 m a.s.l. for debris-free glaciers.

**Assuming an equilibrium line altitude of 5400 m a.s.l. (Sugiyama et al., 2013; Ragetti et al., 2015)

4 Table 2. Remote-sensing data used

Sensor	Date of acquisition	Stereo mode (b/h-ratio)	Spatial/radiometric Resolution	Role
Hexagon KH-9	23 Nov 1974	Stereo (0.4)	6-9m/8-bits	DEM differencing, glacier outlines
Cartosat-1	15 Oct 2006	Stereo (0.62)	2.5m/10-bits	DEM differencing, glacier outlines
Cartosat-1	9 Nov 2009	Stereo (0.62)	2.5m/10-bits	DEM differencing, velocities, glacier outlines
ALOS PRISM	3 Dec 2010	Tri-stereo (0.5)	2.5m/8-bits	DEM differencing, velocities, glacier outlines
SPOT6	21 Apr 2014	Tri-stereo (0.5)	1.5m/12-bits	DEM differencing, glacier outlines
WorldView-2	2 Feb 2015	Stereo (0.5)	0.46m/11-bits	DEM differencing
WorldView-3	22 Feb 2015	Stereo (0.5)	0.31m/11-bits	DEM differencing
SPOT7	7 Mai 2015	Tri-stereo (0.64)	1.5m/12-bits	DEM differencing, glacier outlines
SPOT7	6 Oct 2015	Tri-stereo (0.68)	1.5m/12-bits	DEM differencing
Pléiades	1 and 9 Nov 2014	Across track stereo (0.4)	0.5m/12-bits	Basis for georectification

5

1 Table 3. Mean* uncertainties associated to different sets of elevation change ($\Delta h/\Delta t$) maps.

	No. of maps in category	All glacier area	Debris-covered glacier area
All $\Delta h/\Delta t$ maps, $\Delta t < 4$ a	9	1.18 m a ⁻¹	0.47 m a ⁻¹
All $\Delta h/\Delta t$ maps, $4 \text{ a} \leq \Delta t < 10$ a	12	0.29 m a ⁻¹	0.12 m a ⁻¹
All $\Delta h/\Delta t$ maps involving Hexagon 1974 DEM	7	0.07 m a ⁻¹	0.03 m a ⁻¹
DEM involved, $4 \text{ a} \leq \Delta t < 10$ a			
Cartosat-1 Oct 2006	5	0.22 m a ⁻¹	0.09 m a ⁻¹
Cartosat-1 Nov 2009	4	0.29 m a ⁻¹	0.11 m a ⁻¹
ALOS-PRISM Dec 2010	4	0.43 m a ⁻¹	0.19 m a ⁻¹
SPOT6 April 2014	2	0.24 m a ⁻¹	0.09 m a ⁻¹
WorldView Feb 2015	3	0.32 m a ⁻¹	0.14 m a ⁻¹
SPOT7 May 2015	3	0.31 m a ⁻¹	0.12 m a ⁻¹
SPOT7 October 2015	3	0.24 m a ⁻¹	0.10 m a ⁻¹

* Uncertainties associated to individual maps are shown in Table S1

2 Table 4. Elevation changes of debris-covered glacier tongues due to avalanches triggered by
 3 the Nepal earthquake on 25 April 2015. The first three data columns provide the volume
 4 changes of avalanche affected area divided by the total debris-cover area (Table 1).

	21 Apr 2014- 25 Apr 2015* (m)	25 Apr 2015- 7 May 2015 (m)	25 Apr 2015- 6 Oct 2015 (m)	6 Oct 2015, volume remaining (%)
Langtang**	-0.10 ±0.05	1.33 ±0.42	0.42 ±0.20	31.3%
Langshisha	-0.04 ±0.05	0.32 ±0.37	0.10 ±0.19	31.6%
Shalbachum	-0.11 ±0.05	0.74 ±0.35	0.31 ±0.20	42.5%
Lirung	-0.87 ±0.06	6.79 ±0.38	3.87 ±0.23	57.0%
Average	-0.13 ±0.05	1.31 ±0.35	0.52 ±0.19	39.5%

*Estimation based on average annual melt Oct 2006 – Apr 2014

**Only lower part (south of 28°19'N), upper part not on April 2014 scene

5

6

1 Table 5. Glacier volume and mass changes 1974-2006, ensemble mean 2006-2015*.

	Average elevation differences (m a ⁻¹)		Average mass balance (m w.e. a ⁻¹)	
	Nov1974- Oct2006	Ensemble mean* 2006-2015	Nov1974-Oct2006	Ensemble mean* 2006-2015
Glaciers				
Langtang	-0.28 ± 0.08	-0.55 ± 0.13	-0.24 ± 0.08	-0.47 ± 0.13
Langshisha	-0.12 ± 0.09	-0.45 ± 0.19	-0.10 ± 0.08	-0.38 ± 0.18
Shalbachum	-0.43 ± 0.08	-0.53 ± 0.19	-0.36 ± 0.09	-0.45 ± 0.18
Lirung	-0.17 ± 0.13	-0.22 ± 0.16	-0.14 ± 0.11	-0.19 ± 0.14
Ghanna	-0.51 ± 0.05	-0.46 ± 0.43	-0.43 ± 0.07	-0.39 ± 0.36
Kimoshung	0.07 ± 0.13	-0.02 ± 0.17	0.05 ± 0.10	-0.02 ± 0.13
Yala	-0.33 ± 0.06	-0.89 ± 0.23	-0.28 ± 0.07	-0.76 ± 0.24
Average	-0.24 ± 0.08	-0.45 ± 0.18	-0.21 ± 0.08	-0.38 ± 0.17
Debris-covered areas				
Langtang	-0.79 ± 0.03	-0.91 ± 0.05	-0.67 ± 0.07	-0.78 ± 0.10
Langshisha	-0.69 ± 0.03	-1.16 ± 0.23	-0.58 ± 0.07	-0.98 ± 0.25
Shalbachum	-0.78 ± 0.04	-1.30 ± 0.20	-0.66 ± 0.08	-1.10 ± 0.23
Lirung	-1.03 ± 0.05	-1.67 ± 0.59	-0.87 ± 0.10	-1.42 ± 0.56
Ghanna	-0.58 ± 0.03	-0.50 ± 0.20	-0.49 ± 0.06	-0.43 ± 0.19
Average	-0.78 ± 0.03	-1.02 ± 0.18	-0.66 ± 0.07	-0.87 ± 0.20

*Average of 6 overlapping periods between Oct 2006 and Oct 2015 (Figure S4)

2 Table 6. Sensitivity to outlier correction and Equilibrium Line Altitude (ELA) definitions. $\Delta_{2\sigma}$
3 is the difference in results if a 2σ -level is used to define outliers at all area types, instead of a
4 3σ -level above and a 1σ -level below the ELA. The estimated ELA is 5400 m a.s.l. (Sugiyama
5 et al., 2013; Ragetti et al., 2015). $\Delta_{\text{ELA}\pm 100\text{m}}$ represents the differences in results obtained with
6 an ELA at 5500 m a.s.l. in comparison to results obtained with an ELA at 5300 m a.s.l.

Name	AAR		Elevation differences (m a ⁻¹)			
	ELA -100 m	ELA +100 m	$\Delta_{\text{ELA}\pm 100\text{m}}$	$\Delta_{2\sigma}$	$\Delta_{\text{ELA}\pm 100\text{m}}$	$\Delta_{2\sigma}$
1 Langtang	61%	43%	0.02	-0.01	-0.01	0.01
2 Langshisha	60%	45%	0.06	-0.09	0.02	-0.02
3 Shalbachum	60%	37%	-0.23	0.08	0.04	-0.02
4 Lirung	52%	46%	-0.01	0.01	0.05	-0.01
5 Ghanna	20%	12%	-0.01	0.02	0.00	0.04
6 Kimoshung	88%	80%	0.07	0.06	0.05	-0.16
7 Yala	70%	13%	-0.13	-0.04	-0.11	0.02
All Glacier Area	61%	44%	0.00	-0.01	0.02	-0.01

Sensitivity values that exceed uncertainty ranges as indicated in Table 5 are printed in bold letters.

7
8

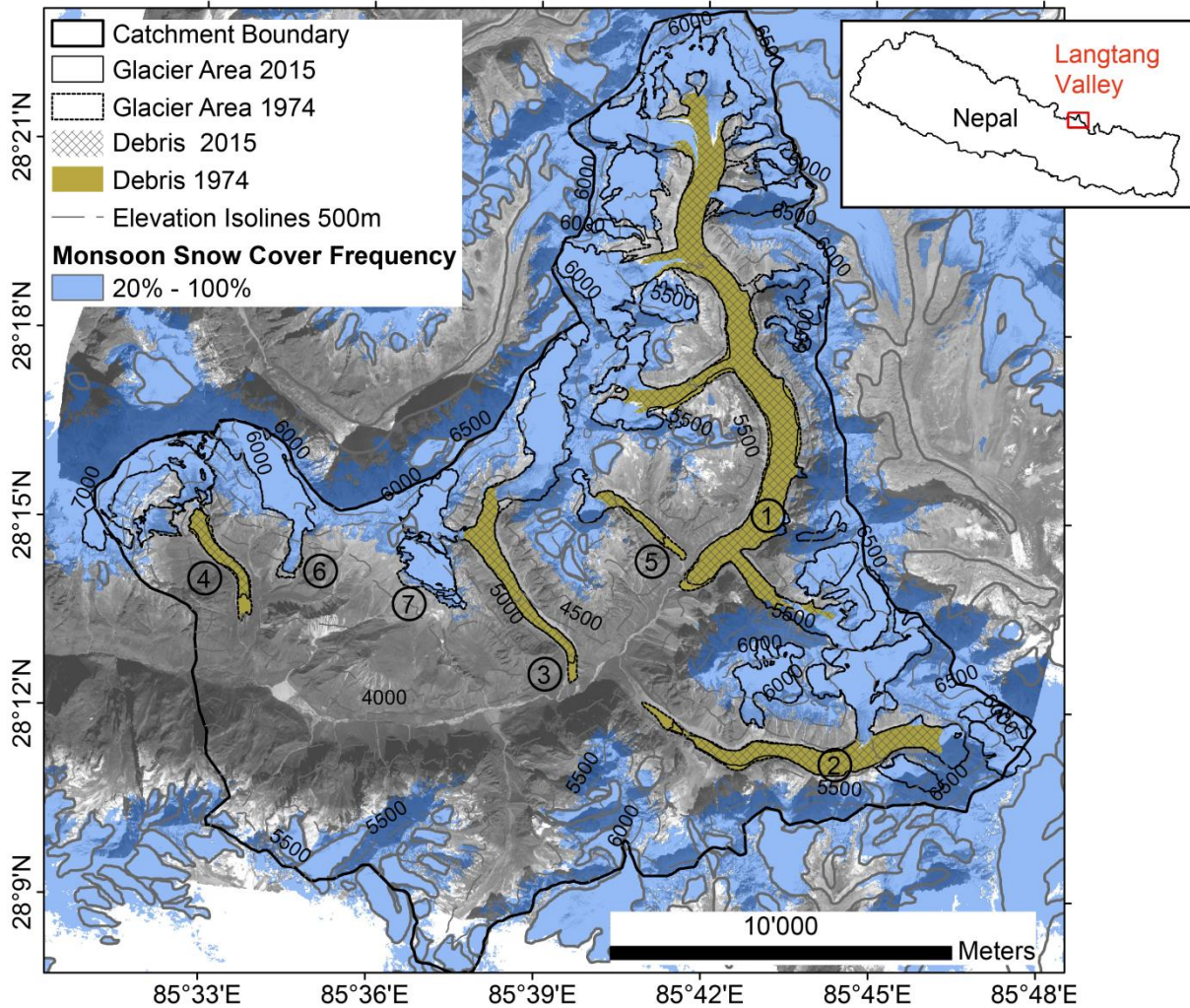
1 **Table 7. Glacier area changes over the periods 1974-2006 and 2006-2015.**

ID	Glacier name	1974-2006		2006-2015	
		km ²	% a ⁻¹	km ²	% a ⁻¹
1	Langtang	-2.65 ± 0.03	-0.17 ± 0.01	-0.45 ± 0.07	-0.11 ± 0.02
2	Langshisha	-0.48 ± 0.09	-0.09 ± 0.02	-0.13 ± 0.05	-0.09 ± 0.04
3	Shalbachum	-0.28 ± 0.06	-0.08 ± 0.02	-0.03 ± 0.04	-0.04 ± 0.04
4	Lirung	-0.45 ± 0.08	-0.20 ± 0.03	-0.05 ± 0.05	-0.08 ± 0.08
5	Ghanna	-0.16 ± 0.03	-0.33 ± 0.05	-0.05 ± 0.01	-0.40 ± 0.12
6	Kimoshung	-0.11 ± 0.01	-0.08 ± 0.01	-0.02 ± 0.01	-0.05 ± 0.02
7	Yala	-0.31 ± 0.03	-0.43 ± 0.05	-0.31 ± 0.03	-1.77 ± 0.16

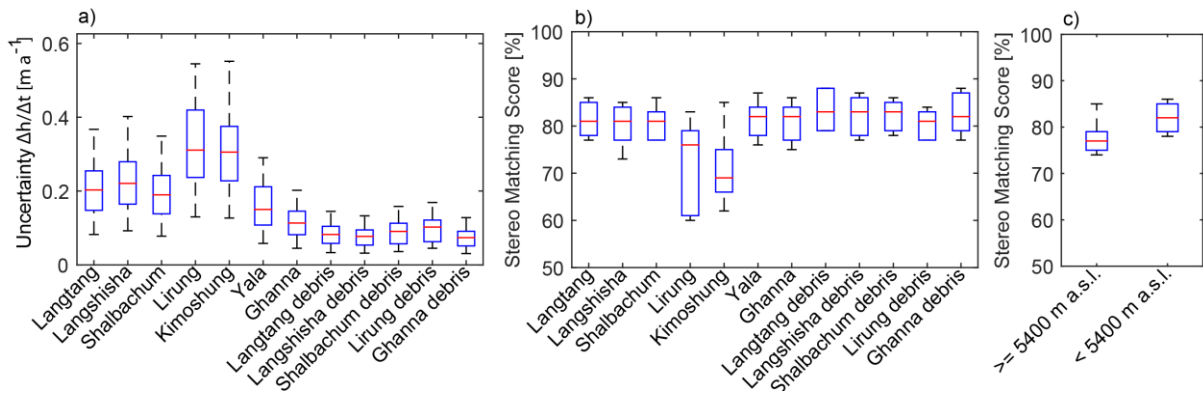
2 **Table 8. Characteristics of the debris-covered tongues (debris-covered glacier area excluding**
 3 **tributary branches).**

	Cliff Area	Lake Area	Mean velocity	% stagnant
Langtang	10.0%	3.3%	5.9 m a ⁻¹	31%
Langshisha	10.5%	2.3%	7.0 m a ⁻¹	20%
Shalbachum	10.3%	2.6%	5.4 m a ⁻¹	29%
Lirung	8.0%	2.3%	2.8 m a ⁻¹	48%
Ghanna	3.2%	0.4%	1.6 m a ⁻¹	85%

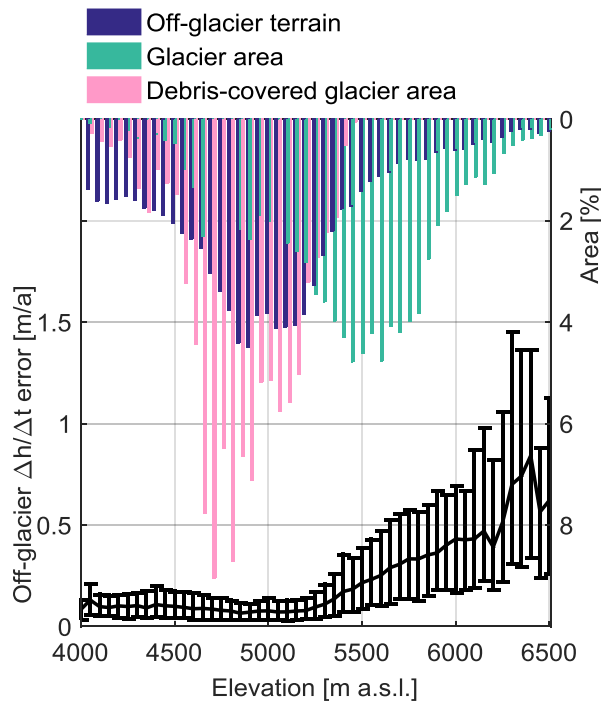
Cliff and lake area corresponds to the percentage of 30-m pixels containing cliffs/lakes (median of 6 available cliff and lake maps from the period 2006-2015). Mean velocity is calculated on the basis of 2009-2010 surface velocities (Figure 13). To discriminate moving ice from quasi-stagnant ice we use a threshold of 2.5 m a⁻¹ (cf. Scherler et al., 2011b), which also corresponds to the approximate uncertainty of remote-sensing derived surface velocity.



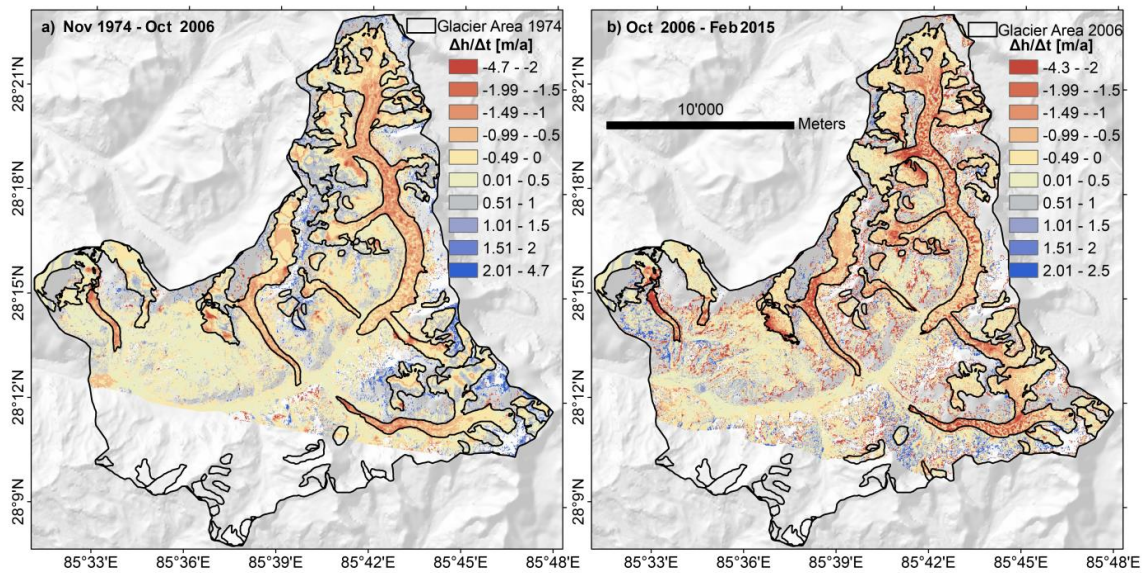
1
 2 Figure 1. Map of the upper Langtang catchment. The numbers on the map correspond to the
 3 glaciers listed in Table 1. Monsoon snow-cover frequency is based on Landsat 1999 to 2013
 4 land cover classifications (Miles et al., 2016b). 1974 glacier area (dotted lines) is shown for
 5 the seven studied glaciers only.
 6



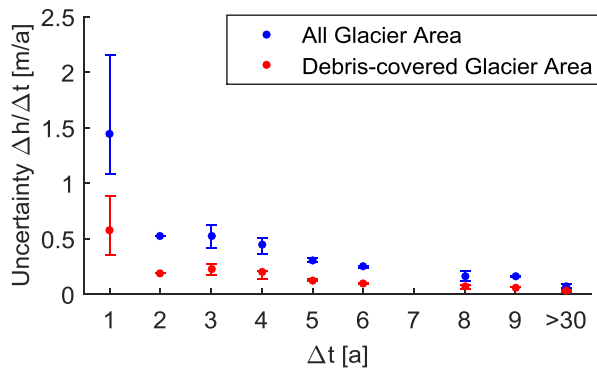
1
 2 Figure 2. a) Uncertainty estimates of average elevation change rates ($\Delta h/\Delta t$) per individual
 3 glacier and per debris-covered tongue. The central mark is the median of the ensemble ($\Delta h/\Delta t$
 4 maps that are rejected according to Section 3.2.5 are excluded). b) Ensemble of stereo
 5 matching scores per individual glacier and debris-covered tongue and c) per glacier area
 6 above and below the estimated ELA. The central marks correspond to the median of all
 7 DEMs (except Hexagon 1974 and WorldView 2015 DEMs for which matching scores are not
 8 available). The edges of each box are the 25th and 75th percentiles. The whiskers extend to
 9 the most extreme data points.



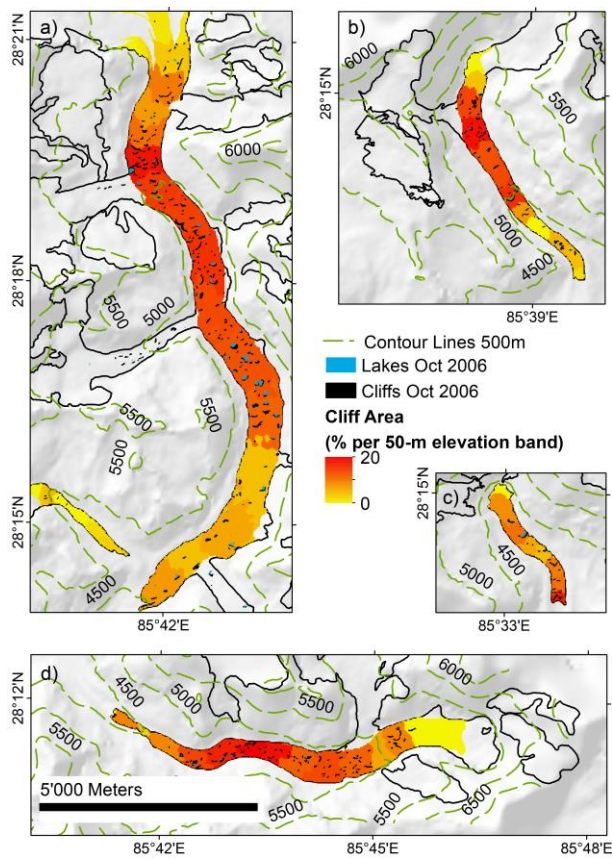
10
 11 Figure 3. Off-glacier elevation change error ($\Delta h/\Delta t$) per 50-m elevation band. The black line
 12 represents the median error in the ensemble of $\Delta h/\Delta t$ maps (excluding $\Delta h/\Delta t$ maps that are
 13 rejected according to Section 3.2.5). Error bars represent 95% confidence intervals.



1
 2 Figure 4. Elevation change rates ($\Delta h/\Delta t$) derived from a) Hexagon Nov 1974 and Cartosat-1
 3 Oct 2006 DEMs and (b) Cartosat-1 Oct 2006 and WorldView Feb 2015 DEMs.



4
 5 Figure 5. Uncertainties in elevation change rates ($\Delta h/\Delta t$) in function of the time interval
 6 between DEMs (Δt). Median results of all available 28 $\Delta h/\Delta t$ maps. Error bars extend to the
 7 most extreme data points.



1
 2 Figure 6. Supraglacial cliffs and lakes as identified from the Oct 2006 Cartosat-1 satellite
 3 image: a) Langtang and Ghanna Glaciers, b) Shalbachum Glacier, c) Lirung Glacier, d)
 4 Langshisha Glacier. Cliff area shows the median fraction (%) of 30-m pixels per 50m
 5 elevation band that contain cliffs, considering all 6 available cliff maps from 2006-2015.

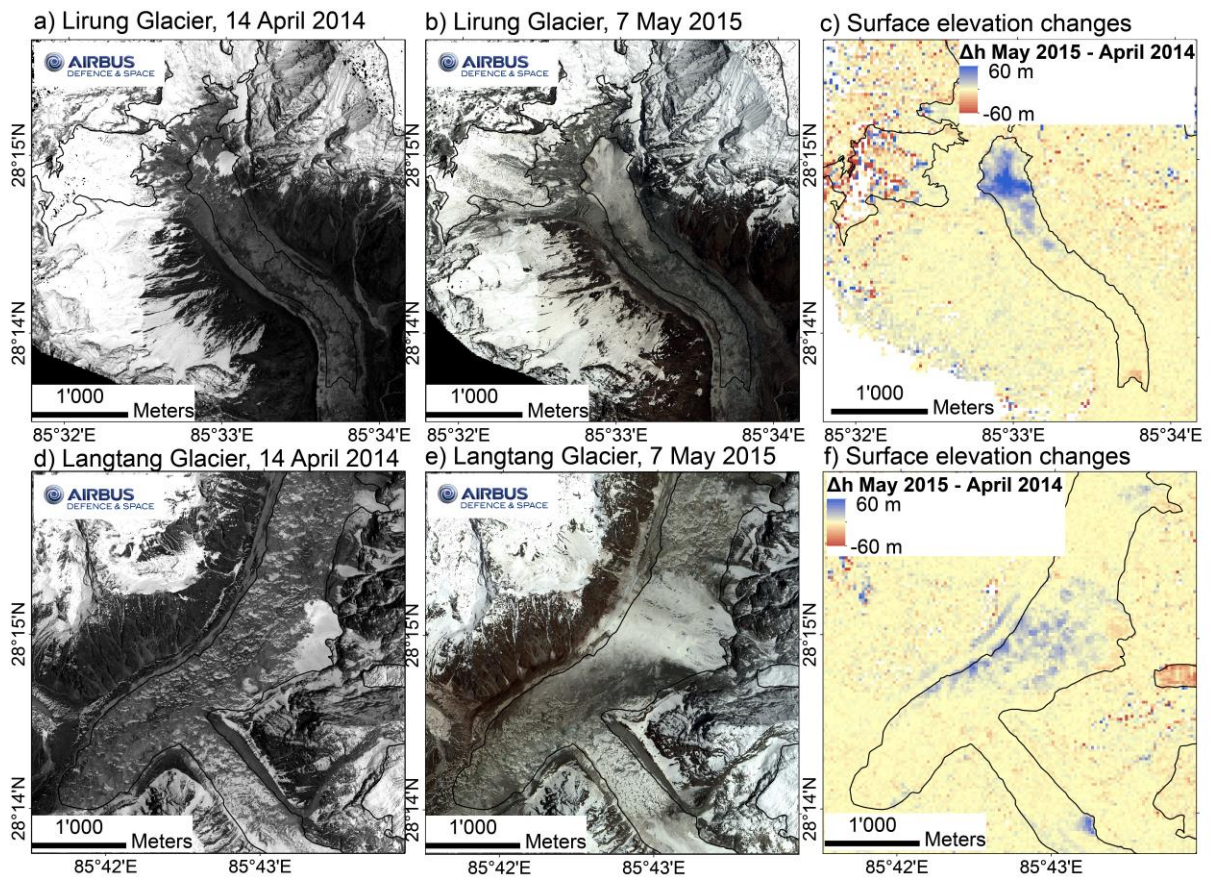
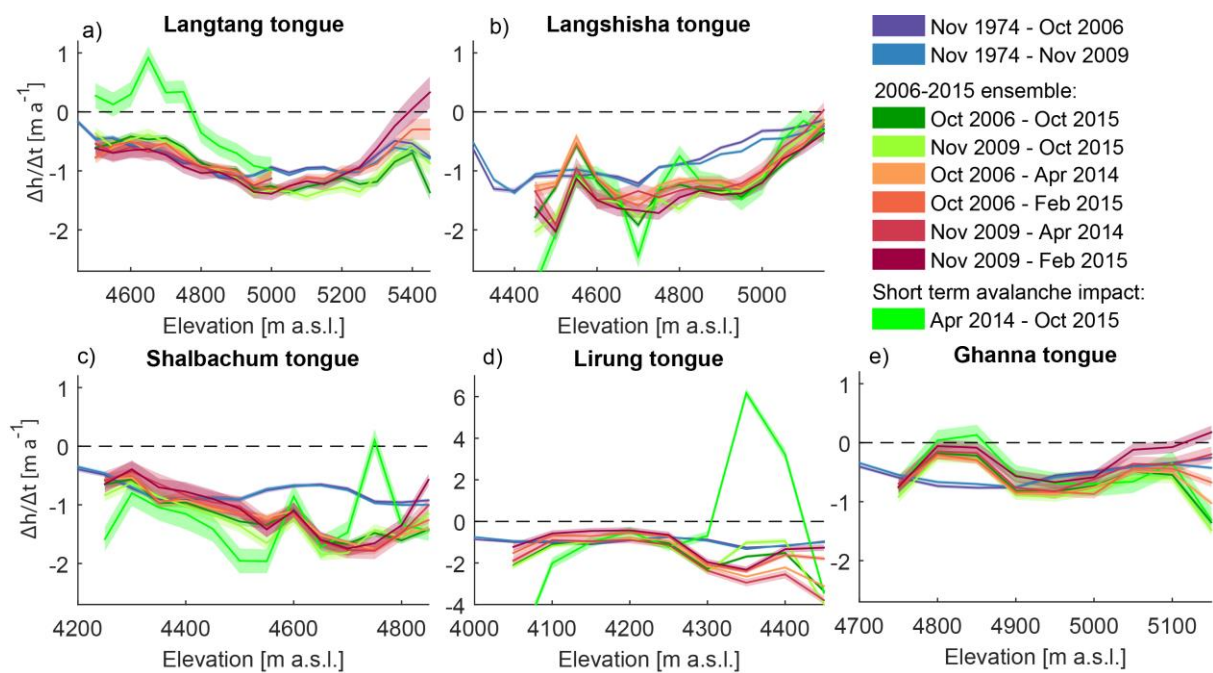
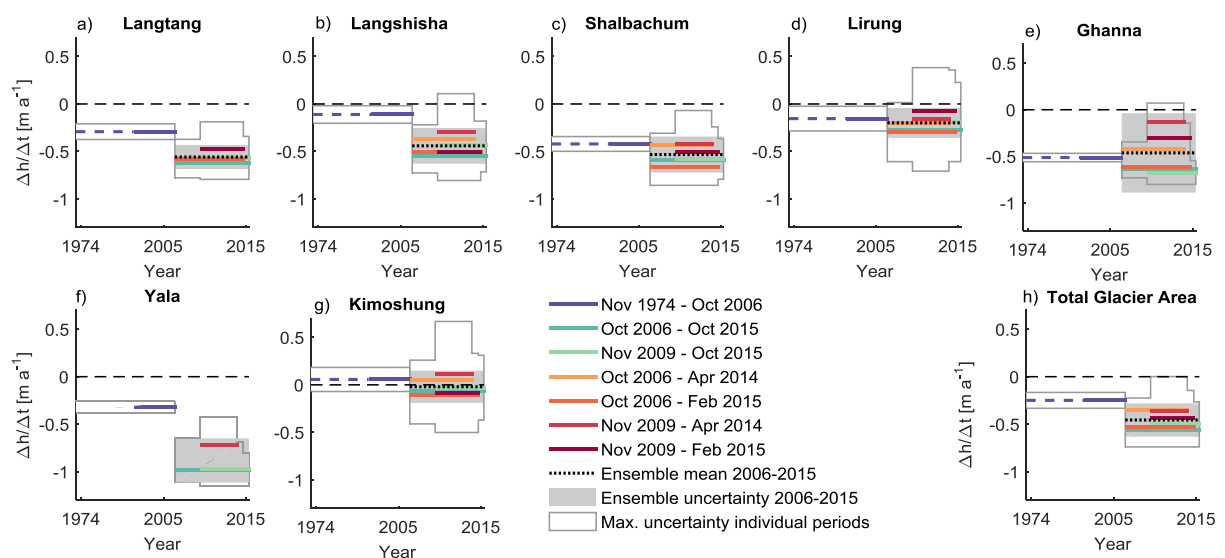


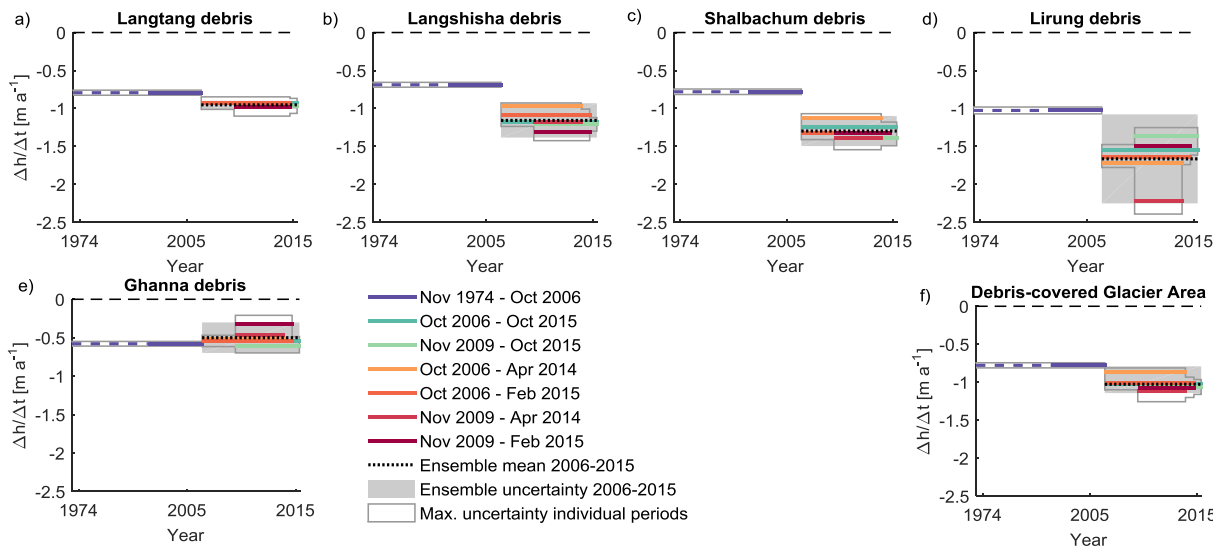
Figure 7. Avalanche affected sections of Lirung and Langtang glacier, pre- and after the earthquake on 25 April 2015, and corresponding surface elevation changes (Δh). Imagery ©Airbus DS 2014/2015.



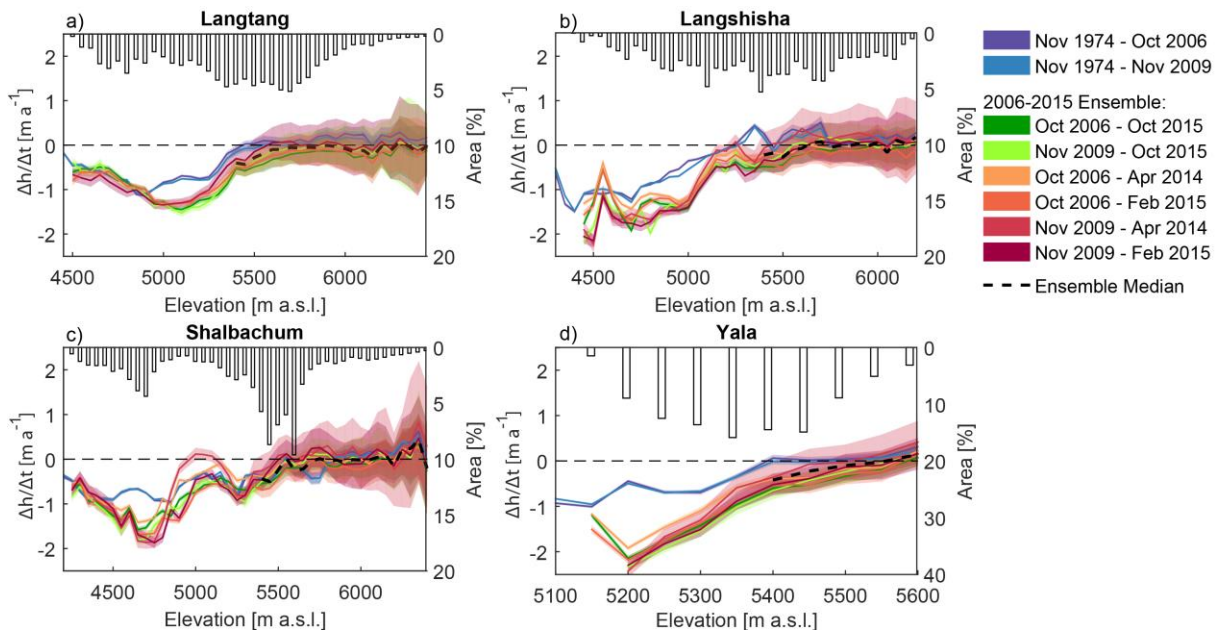
1
 2 Figure 8. Altitudinal distribution of mean annual elevation change ($\Delta h/\Delta t$) over 50 m
 3 elevation bands of debris-covered tongues (debris-covered area of each glacier excluding
 4 tributary branches). Uncertainty bounds correspond to uncertainty in function of elevation
 5 derived for each $\Delta h/\Delta t$ map individually (Figure 3).



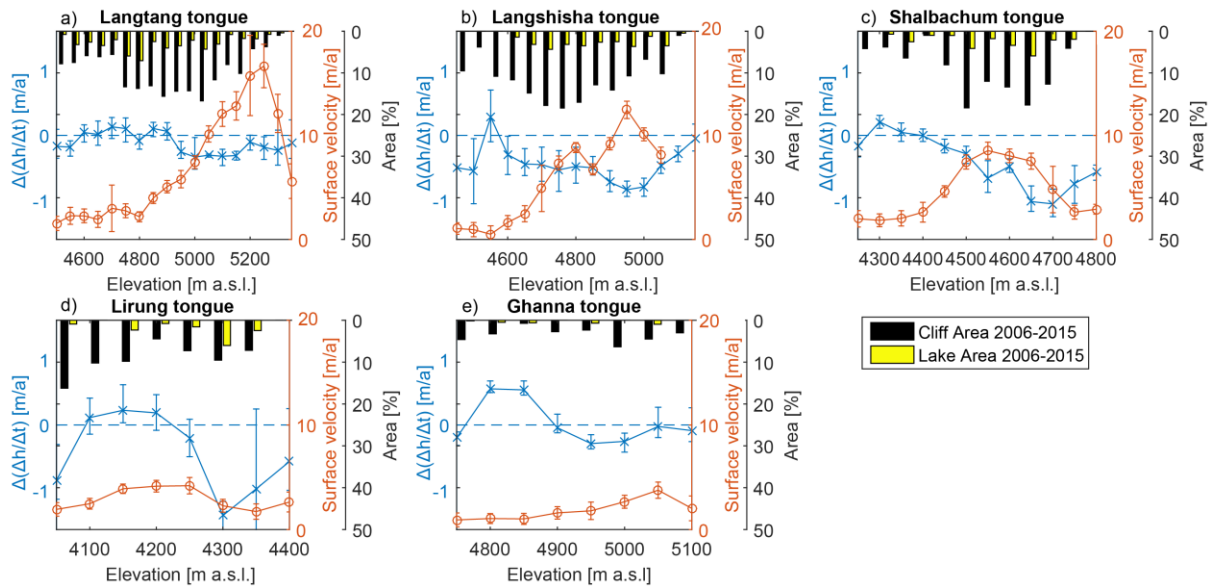
6
 7 Figure 9. Mean elevation change rates ($\Delta h/\Delta t$) per period and glacier. For better readability,
 8 only the maximum width of error bounds corresponding to individual periods 2006-2015 are
 9 shown.



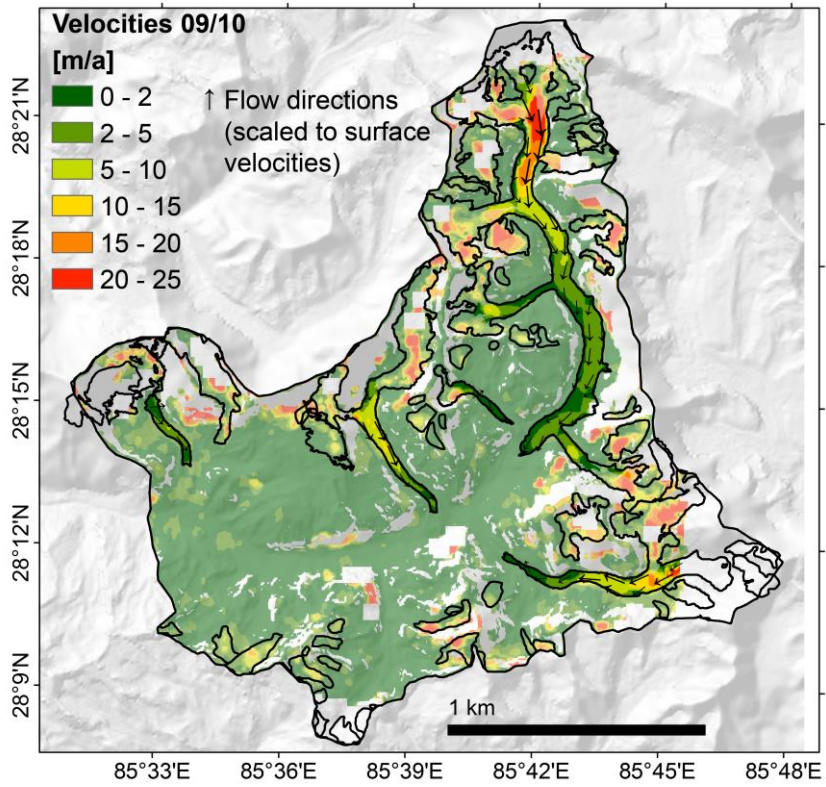
1
 2 Figure 10. Mean elevation change rates ($\Delta h/\Delta t$) per period and debris-covered glacier area.
 3 For better readability, only the maximum width of error bounds corresponding to individual
 4 periods 2006-2015 are shown.



5
 6 Figure 11. Altitudinal distribution of mean annual elevation change ($\Delta h/\Delta t$) and altitudinal
 7 distribution of glacier area (%) over 50 m elevation bands of selected glaciers. Uncertainty
 8 bounds correspond to uncertainty in function of elevation derived for each $\Delta h/\Delta t$ map
 9 individually (Figure 3). Ensemble median values shown here are used to replace missing data
 10 in the accumulation areas of glaciers after outlier exclusion (Section 3.2.3). Note that the
 11 x-axis ranges are different for each sub-figure.



1
 2 Figure 12: Altitudinal distribution of cliff and lake area fractions, glacier velocity and changes
 3 in thinning rates. Cliff and lake area is shown as % of 30-m pixels containing cliffs/lakes per
 4 50 m elevation band, whereas the values represent the median of 6 available cliff and lake
 5 maps from the period 2006-2015. Glacier velocities (m/a) represent the median per 50 m
 6 elevation band of data shown in Figure 11 and error bars represent the standard deviation in
 7 pixel values per elevation band. Changes in thinning rates ($\Delta(\Delta h/\Delta t)$ [m/a]) are calculated
 8 comparing 1974-2006 and the 2006-2015 ensemble-mean. Negative $\Delta(\Delta h/\Delta t)$ values
 9 represent thinning accelerations. Error bars represent the maximum variations in $\Delta(\Delta h/\Delta t)$
 10 considering all individual periods within the 2006-2015 ensemble.



1
2 Figure 13: Surface velocities 2009-2010 cropped to catchment boundaries. Values have units
3 of meters per year and are derived by cross-correlation feature tracking. Off-glacier velocities
4 are shown in transparent color.
5